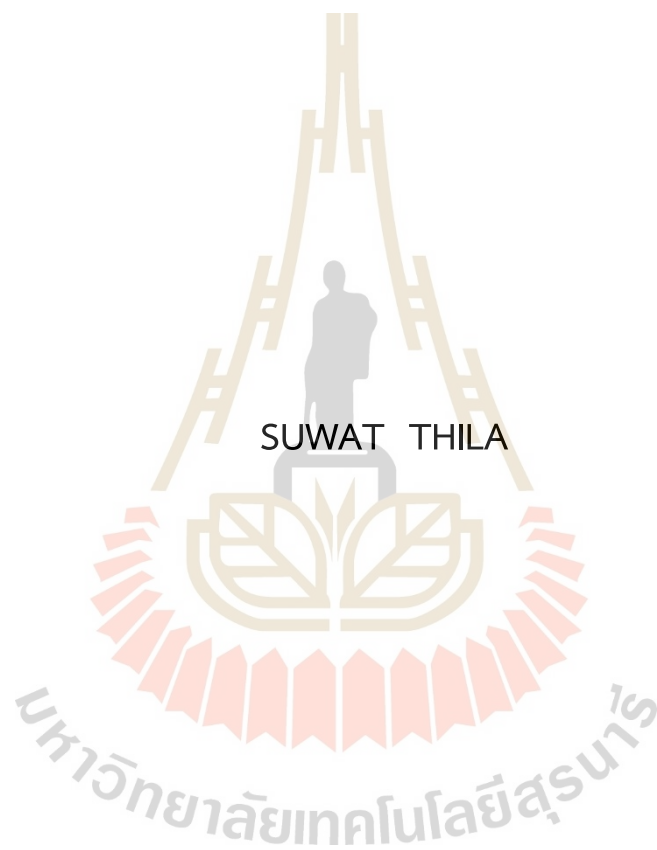


THE OXIDATION REACTIVITY AT SURFACE OF HAFNIUM  
DISELENIDE IN VACUUM AND ATMOSPHERIC PRESSURE  
ENVIRONMENT



A Thesis Submitted in Partial Fulfillment of the Requirement for the  
Degree of Master of Science in Physics  
Suranaree University of Technology  
Academic Year 2021

ปฏิบัติการออกซิเดชันที่พื้นผิวของแอฟเนียมไดเซเลไนต์ในสภาวะสุญญากาศ  
และความดันบรรยากาศ



วิทยานิพนธ์นี้เป็นส่วนหนึ่งของการศึกษาตามหลักสูตรปริญญาวิทยาศาสตรมหาบัณฑิต  
สาขาวิชาฟิสิกส์  
มหาวิทยาลัยเทคโนโลยีสุรนารี  
ปีการศึกษา 2564

THE OXIDATION REACTIVITY AT SURFACE OF HAFNIUM DISELENIDE IN  
VACUUM AND ATMOSPHERIC PRESSURE ENVIRONMENT

Suranaree University of Technology has approved this thesis submitted in partial fulfillment of the requirements for a Master's degree.

Thesis Examining Committee



(Assoc. Prof. Dr. Prayoon Songsiritthigul)

Chairperson



(Assoc. Prof. Dr. Worawat Meevasana)

Thesis Advisor



(Dr. Chanan Euaruksakul)

Member



(Dr. Narong Chanlek)

Member



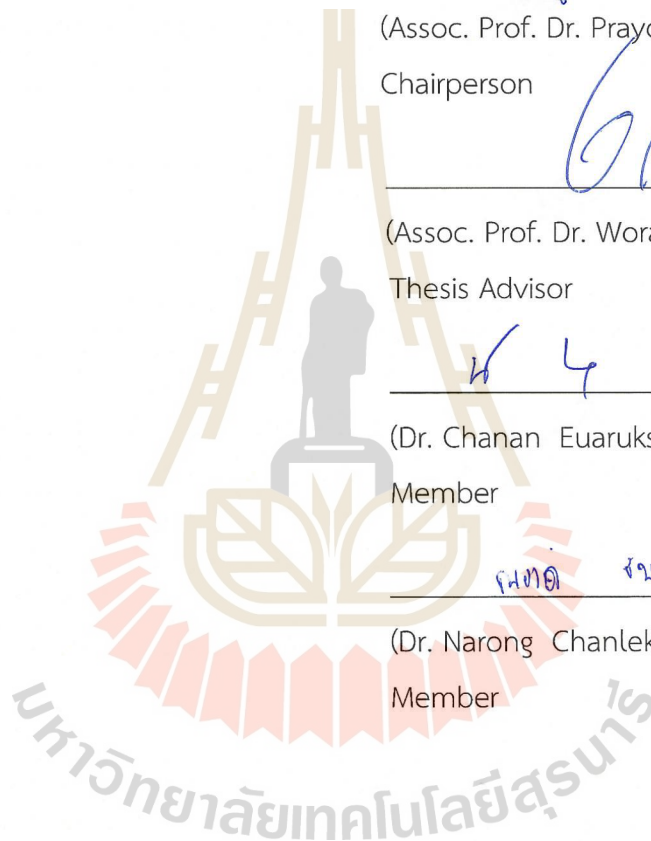
(Assoc. Prof. Dr. Yupaporn Ruksakulpiwat)

Vice Rector for Academic Affairs  
and Quality Assurance



(Prof. Dr. Santi Maensiri)

Dean of Institute of Science



SUWAT THILA : THE OXIDATION REACTIVITY AT SURFACE OF HAFNIUM  
DISELENIDE IN VACUUM AND ATMOSPHERIC PRESSURE ENVIRONMENT.  
THESIS ADVISOR : ASSOC. PROF. WORAWAT MEEVASANA, Ph.D. 54 PP.

Keyword: HAFNIUM DISELENIDE ( $\text{HfSe}_2$ )/PHOTOEMISSION ELECTRON MICROSCOPY (PEEM)/  
X - RAY PHOTOEMISSION SPECTROSCOPY (XPS)

Hafnium Diselenide ( $\text{HfSe}_2$ ) is an ideal semiconductor for electronic applications because of its high carrier mobility and proper bandgap but there is a limitation that the surface is sensitive under the ambient condition and can be oxidized easily. However, the oxidation of  $\text{HfSe}_2$  can cause Hafnium dioxide ( $\text{HfO}_2$ ) which is a high dielectric material.

In this thesis, the chemical composition as a function of depth profile of 1-day air exposure  $\text{HfSe}_2$  sample is observed by using x-ray photoemission spectroscopy. By non-destructive measurement of the sample by changing the angle, the results show that  $\text{HfO}_2$  is highest in the upper layer of  $\text{HfSe}_2$  and decreases relatively with depth. The forming Se-Se has the highest amount in the upper layer of the  $\text{HfSe}_2$  surface as well. Hf-O and Se-Se are eliminated from the surface by destructive measurement using Argon sputtering, but Hf Suboxide ( $\text{Hf}^{\text{ox}}$ ) appears after sputtering.

the oxidation effects on exfoliated flakes of  $\text{HfSe}_2$  are studied under different conditions which are  $\text{O}_2$  and  $\text{H}_2\text{O}$  exposure in vacuum, ambient and  $95\pm 5\%$  relative humidity (RH) exposure at atmospheric pressure. The results of the study using photoemission electron microscopy (PEEM) with in-situ measurements show that  $\text{H}_2\text{O}$  and  $\text{O}_2$  can cause surface oxidation, from  $\text{HfSe}_2$  to  $\text{HfO}_2$ , with  $\text{O}_2$  exposure resulting in stronger oxidation than  $\text{H}_2\text{O}$  exposure. The effects of  $\text{H}_2\text{O}$  and  $\text{O}_2$  exposure with relative humidity of  $95\pm 5\%$  at atmospheric pressure for 4 hours fully oxidize the surface and Se-Se bonding is formed after the oxidation. The work function mapping of  $\text{HfSe}_2$  that is exposed to different conditions shows that the contrast remains after being exposed. Although it becomes less apparent as exposure time increases, the persistence of work function contrast is different for each condition. As a result, we suggest that

the difference in oxidation behavior and the difference in work function contrast are both related behaviors that appear to be connected.

The understanding of the oxidation reactivity at the surface of  $\text{HfSe}_2$  will leads to the method for controlling and growth homogenous oxide  $\text{HfSe}_2/\text{HfO}_2$  interfaces for creating a good quality Transition-metal dichalcogenide (TMD)/high -  $\kappa$  dielectric gate insulators in Field-Effect Transistors (FETs).



School of Physics  
Academic Year 2021

Student's Signature

Advisor's Signature



สุวัฒน์ ธิหล้า : ปฏิกริยาออกซิเดชันที่พื้นผิวของแฮฟเนียมไดเซเลไนด์ในสภาวะสุญญากาศ และความดันบรรยากาศ (THE OXIDATION REACTIVITY AT SURFACE OF HAFNIUM DISELENIDE IN VACUUM AND ATMOSPHERIC PRESSURE ENVIRONMENT).

อาจารย์ที่ปรึกษา : รองศาสตราจารย์ ดร.วรวัดน์ มีวาสนา, 54 หน้า.

คำสำคัญ: แฮฟเนียมไดเซเลไนด์ ( $\text{HfSe}_2$ )/กล้องจุลทรรศน์ของโพโตมิชชันของอิเล็กตรอน/เทคนิคสเปกโทรสโกปีโพโตอิเล็กตรอนด้วยรังสีเอกซ์

แฮฟเนียมไดเซเลไนด์ (Hafnium Diselenide :  $\text{HfSe}_2$ ) เป็นสารกึ่งตัวนำตัวเลือกหนึ่งที่เหมาะสมสำหรับการใช้งานทางอิเล็กทรอนิกส์ เนื่องด้วยประจุพาหะมีความสามารถในการเคลื่อนที่สูง และมีช่องว่างระหว่างแถบพลังงานที่เหมาะสม อย่างไรก็ตามยังมีข้อจำกัดในการนำไปใช้งานเนื่องจากพื้นผิวมีความไวต่อการเกิดปฏิกิริยาภายใต้สภาวะแวดล้อมโดยรอบและสามารถออกซิไดซ์ได้ง่าย แต่การออกซิไดซ์ของ  $\text{HfSe}_2$  จะทำให้เกิด แฮฟเนียมไดออกไซด์ (Hafnium dioxide :  $\text{HfO}_2$ ) ซึ่งเป็นสารที่มีค่าไดอิเล็กทริกสูง

ในวิทยานิพนธ์นี้ได้ศึกษาองค์ประกอบทางเคมีตามระดับความลึกจากเทคนิคสเปกโทรสโกปีโพโตอิเล็กตรอนด้วยรังสีเอกซ์ของแฮฟเนียมไดเซเลไนด์ที่ลอกเป็นแผ่นบางที่สัมผัสกับอากาศเป็นเวลา 1 วัน โดยวิธีการวัดแบบไม่ทำลายตัวอย่างด้วยการเปลี่ยนแปลงมุมพบว่า  $\text{HfO}_2$  จะมีปริมาณสูงสุดบริเวณชั้นบนของผิว  $\text{HfSe}_2$  และลดลงตามระดับความลึก ส่วน Se-Se ที่เกิดขึ้นจะมีปริมาณสูงสุดบริเวณชั้นบนของผิว  $\text{HfSe}_2$  เช่นเดียวกัน ส่วนวิธีการวัดแบบทำลายตัวอย่างด้วยการใช้อาร์กอนไอออนสปัตเตอร์ริงนั้นจะทำให้ Hf-O และ Se-Se ถูกกำจัดออกไปแต่จะเกิดแฮฟเนียมซบออกไซด์ ( $\text{HF}^+$ ) เกิดขึ้นหลังจากสปัตเตอร์ริง

การศึกษาปฏิกิริยาออกซิเดชันที่พื้นผิวของ  $\text{HfSe}_2$  ที่ลอกเป็นแผ่นบางในเงื่อนไขที่แตกต่างกัน กล่าวคือ สัมผัสกับ  $\text{O}_2$  ในสุญญากาศ, สัมผัสกับ  $\text{H}_2\text{O}$  ในสุญญากาศ, สัมผัสกับอากาศที่ความดันบรรยากาศ และ สัมผัสกับอากาศที่มีความชื้นสัมพัทธ์  $95\pm 5\%$  ที่ความดันบรรยากาศ ซึ่งผลการศึกษาโดยใช้เทคนิคกล้องจุลทรรศน์ของโพโตมิชชันของอิเล็กตรอนด้วยการวัดแบบอินซิทู พบว่า  $\text{H}_2\text{O}$  และ  $\text{O}_2$  ทั้งสองเป็นสาเหตุของการเกิดออกซิเดชันบนพื้นผิว  $\text{HfSe}_2$  เป็น  $\text{HfO}_2$  โดยการสัมผัสกับ  $\text{O}_2$  จะส่งผลให้เกิดการออกซิไดซ์ที่รุนแรงกว่าการสัมผัสกับ  $\text{H}_2\text{O}$  ซึ่งผลการทำงานร่วมกันระหว่าง  $\text{H}_2\text{O}$  และ  $\text{O}_2$  ภายใต้เงื่อนไขในการสัมผัสกับอากาศที่มีความชื้นสัมพัทธ์  $95\pm 5\%$  ในความดันบรรยากาศเป็นเวลา 4 ชั่วโมงจะเกิดการออกซิไดซ์อย่างเต็มที่บนพื้นผิว โดยเมื่อเกิดการออกซิไดซ์บนพื้นผิวของ  $\text{HfSe}_2$  ไปเป็น  $\text{HfO}_2$  จะส่งผลให้เกิดพันธะ Se-Se เกิดขึ้นหลังจากการออกซิไดซ์

การทำแผนที่พลังงานยึดเหนี่ยว (work function mapping) บนพื้นผิวของ  $\text{HfSe}_2$  ที่สัมผัสกับสถานะต่าง ๆ แสดงให้เห็นว่าคอนทราสต์ยังคงอยู่หลังจากสัมผัส แม้ว่าจมองเห็นได้น้อยลงเมื่อเวลานานขึ้น แต่ความคงอยู่ของคอนทราสต์ในแผนที่พลังงานยึดเหนี่ยวจะแตกต่างกันไปในแต่ละสถานะที่สัมผัส ด้วยเหตุนี้ เราจึงสังเกตได้ว่าความแตกต่างของพฤติกรรมการออกซิเดชันและความแตกต่างของคอนทราสต์ในแผนที่พลังงานยึดเหนี่ยวเป็นพฤติกรรมที่เกี่ยวข้องกันซึ่งดูเหมือนจะเชื่อมโยงกัน

การเข้าใจปฏิกิริยาออกซิเดชันที่พื้นผิวของ  $\text{HfSe}_2$  จะนำไปสู่วิธีการควบคุมและสร้างชั้นต่อประสานระหว่าง  $\text{HfSe}_2$  กับ  $\text{HfO}_2$  สำหรับการสร้างชั้นต่อประสานระหว่างโลหะทรานซิชันไดคัลโคเจไนด์ (Transition-metal dichalcogenide: TMD) กับ ฉนวนเกตที่มีค่าไดอิเล็กทริกสูง (high-dielectric gate insulators) ที่คุณภาพดีในทรานซิสเตอร์สนามไฟฟ้า



สาขาวิชาฟิสิกส์  
ปีการศึกษา 2564

ลายมือชื่อนักศึกษา \_\_\_\_\_  
ลายมือชื่ออาจารย์ที่ปรึกษา \_\_\_\_\_

## ACKNOWLEDGEMENTS

The completion of my thesis would not have been possible without the help of many people. To begin, I would like to express my gratitude to Associate Professor Dr. Worawat Meevasana, who served as my thesis adviser. Going back in time when I was a senior student, I wanted to learn about synchrotron radiation techniques. I'm trying to find a advisor to teach me during a cooperative education program. That is the reason that I met him for the first time. Over this time, he opened my eyes to a lot of scientific perspectives that I've never looked at before. This makes me very impressed with him. I decided to move from Phitsanulok to Nakhon Ratchasima to study for a master's degree with him after completing my bachelor's degree. I have been a member of his research group for about 5 years. My time right now is quite valuable to me. He provided me a large chance to do the experiment in China, which is my valuable experience, and this is my first time abroad. He is a really kind and helpful advisor. I am thankful to him for his support in supervising and providing knowledge in the resolution of this thesis.

I would like to acknowledge Assoc. Prof. Dr. Prayoon Songsiritthigul, Dr. Chanan Euaruksakul and Dr. Narong Chanlek for giving their valuable time to be the thesis defense committee and providing helpful feedback about my work.

I am grateful to everyone at Beamlines 3.2b and 5.3 the Synchrotron Light Research Institute (SLRI) for their support in performing the experiments.

I am fortunate to meet every member of Meevasana group. I would like to thank Dr. Tanachat Eknapakul, Dr. Sumet Siriroj, Dr. Siwat Polin and Dr. Supansa Musikajaroen, Dr. Worasarit Saengsui, Dr. Sujinda Chaiyachad, Dr. Peerawat Laohana, Dr. Warakorn Jindata Mr. Seksan Laopa, Mr. Suppanat Sangphet, Ms. Aissara Rasritat, Ms. Areeya Mooltang, Mr. Ukrit Jitropas, Mr. Anan Sutcha, Ms. Pakwan Chaprakhon, Mr. Yattiphon Kaeokhamchan and Mr. Chonnarong Kaewsai for their help, kindness, entertainment and valuable friendship.

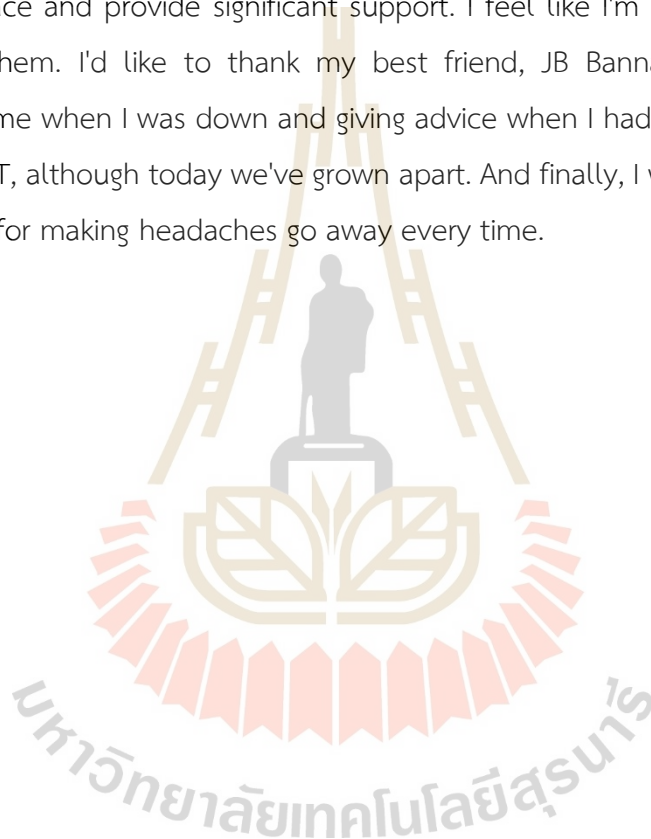


I am thankful to all the instructors and staff at the School of Physics, Institute of Science, and Suranaree University of Technology for their support.

I would like to acknowledge the Development and Promotion of Science and Technology Talents Project (DPST) scholarship for financial support since I was in a bachelor's degree.

I would like to express my appreciation to both my family and my friends. First and foremost, I want to express my gratitude to my parents, who always give me a hearty embrace and provide significant support. I feel like I'm charging energy every time I call them. I'd like to thank my best friend, JB Bannakit, M.D., for always encouraging me when I was down and giving advice when I had a problem during my studies at SUT, although today we've grown apart. And finally, I want to say thank you to Naproxen for making headaches go away every time.

Suwat Thila



# CONTENTS

	Page
ABSTRACT IN THAI .....	I
ABSTRACT IN ENGLISH .....	III
ACKNOWLEDGEMENTS .....	V
CONTENTS .....	VII
LIST OF TABLES .....	IX
LIST OF FIGURES .....	X
<b>CHAPTER</b>	
<b>I INTRODUCTION .....</b>	<b>1</b>
1.1 Background and motivation.....	1
1.2 Research objectives.....	2
1.3 Outline of thesis .....	3
<b>II LITERATURE REVIEWS .....</b>	<b>4</b>
2.1 HfSe <sub>2</sub> -based transistor.....	4
2.2 The oxidation at surface HfSe <sub>2</sub> after ambient expose.....	6
<b>III RESERCH METHODLOGY .....</b>	<b>15</b>
3.1 Photoemission .....	15
3.2 X-ray photoelectron spectroscopy (XPS).....	17
3.2.1 Inelastic mean free path.....	18
3.2.2 Sampling depth.....	19
3.2.3 XPS depth profiling.....	22
3.3 Photo Electron Emission Microscopy (PEEM).....	23
3.3.1 X - ray photo electron emission spectromicroscopy (XPEEM).....	27
3.3.2 Area probe X-ray Photoelectron Spectroscopy (Area probe-XPS).....	30
3.3.3 Work function measurement and mapping.....	31

## CONTENTS (Continued)

	Page
<b>IV RESULTS AND DISCUSSION .....</b>	<b>37</b>
4.1 The depth profile of Hafnium Diselenide (HfSe <sub>2</sub> ) surface after ambient exposure.....	37
4.1.1 Angle-dependent XPS depth profile .....	37
4.1.2 Argon ion sputtering XPS depth profile .....	39
4.2 The surface oxidation dynamic of Hafnium Diselenide (HfSe <sub>2</sub> ).....	42
4.2.1 PEEM image of Hafnium Diselenide (HfSe <sub>2</sub> ) thin flakes.....	42
4.2.2 Area probe X-ray Photoelectron Spectroscopy (Area probe-XPS).....	42
4.2.3 Work function Mapping .....	44
<b>V CONCLUSION .....</b>	<b>47</b>
5.1 Conclusions .....	47
5.2 Future direction .....	48
REFERENCES .....	49
CURRICULUM VITAE.....	54

## LIST OF TABLES

Table	Page
2.1 The specification and performance of prototype HfSe <sub>2</sub> -base transistors .....	5



## LIST OF FIGURES

Figure	Page
2.1 Degradation of exfoliated HfSe <sub>2</sub> flakes over time on a 285 nm SiO <sub>2</sub> substrate. Optical images (a) after 1 day and (b) after 8 days in ambient conditions. The AFM images after 1 day and 8 days in ambient conditions are shown in (c) and (d), respectively. The black dotted boxes in (a) and (b) represent locations where an AFM scanning image was obtained. (Kang et al., 2015) .....	7
2.2 (a) The HfSe <sub>2</sub> AFM image was taken 24 hours after exfoliation. The cross - section of the tallest protrusion (approximately 60 nm) and a 3D surface feature are shown in the inset. (b) SEM image of HfSe <sub>2</sub> 5 months and 1 day on the inset from exfoliation which shows the same kind of protrusions in terms of form and shape, only smaller. (c) TEM image of the surface blisters on the thick HfSe <sub>2</sub> flake. (Mirabelli et al., 2016).....	8
2.3 Hf 4f peaks XPS spectrum of Hf; freshly cleaved (a), after 1 hour (b), 3 hours (c), and 48 hours (d) ambient exposure and re-cleaving (d). (Gioele Mirabelli et al., 2016).....	9
2.4 Se 3d peaks XPS spectrum of Se; freshly cleaved (a), after 1 hour (b), 3 hours (c), and 48 hours (d) ambient exposure and re-cleaving (d). (Gioele Mirabelli et al., 2016).....	10
2.5 Cross-sectional TEM image of HfSe <sub>2</sub> flake after 7 days of ambient exposure. Insets show EDX elemental mapping revealing complete chalcogen depletion, as seen by the overlap of O and Se signals. The scale bars specify 50 nm. (Mleczko et al., 2017) .....	11
2.6 A comparison of the Raman spectra of HfSe <sub>2</sub> flakes obtained immediately after exfoliation in the air (a), a glove box (b), and after long-term air exposure (c). (Cruz et al., 2018).....	12

## LIST OF FIGURES (Continued)

Figure	Page
2.7 The topography image of MoS <sub>2</sub> (a), WSe <sub>2</sub> (b) and HfSe <sub>2</sub> (c) surfaces, all taken with the same scanning tunneling microscopy conditions (Yao et al., 2018) .....	13
2.8 HfSe <sub>2</sub> oxidation evolution measured with C-AFM at t <sub>0</sub> , t <sub>0</sub> +20 minutes, and t <sub>0</sub> +3 minutes. The bias of the sample is 4.7 V. (Yao et al., 2018).....	13
3.1 Schematic diagram of the excitation process in Photoemission spectroscopy.....	16
3.2 Fitted Hf 4f photoelectron spectrum to indicate the chemical state of HfSe <sub>2</sub> flakes after air exposure and O <sub>2</sub> -plasma treatment. (Liu, 2021).....	18
3.3 The inelastic scattering process in the sample after it has been irradiation with X-rays results in the formation of a kinetic energy distribution (also known as an electron spectrum). (Sowinska., 2014).....	20
3.4 Probability of a photoelectron escaping from a depth d in normal emission geometry. (Sowinska, 2014).....	21
3.5 The conventional (a) and angle dependent XPS at $\alpha = 60^\circ$ (b), $\alpha = 30^\circ$ (c) experimental setup. (Schneider et al., 2005).....	22
3.6 Schematic of the XPS sputtering depth profiling method (Zborowski, 2018).....	23
3.7 The PEEM technique's operating principle .....	24
3.8 The surface features of the topography and their related PEEM image (Stohr and Anders, 2000) .....	26
3.9 A schematic view of the XPEEM. The instrument is performed at the BL3.2Ub in the Synchrotron Light Research Institute (SLRI), Thailand. (Tunmee, 2016).....	27
3.10 A schematic of a photoelectron spectrum displaying the wide range of kinetic energies that may be selected (Barrett and Renault, 2009).....	28
3.11 In the XPEEM imaging mode, the contrast is obtained by utilizing (a) total photoelectron yield and (b) and (c) the energy filter, respectively. (Greiner, 2007) .....	29

## LIST OF FIGURES (Continued)

Figure	Page
3.12 (a) Si 1s and (b) Ag 3d photoelectron energy dispersion spectral) images and their intensity plot profiles. (Yasufuku et al., 2006) .....	30
3.13 Area probe-XPS spectra of Sn 3d <sub>5/2</sub> obtained throughout the whole field of vision (blue) and on the pattern using a 20 μm iris aperture (red). (Renault et al., 2012) .....	31
3.14 A part of the gold survey spectrum obtained with monochromatic Al K-α radiation (Azo materials, 2020) .....	32
3.15 Principle of work function mapping. ....	33
3.16 (a) Energy filtered PEEM image (E-E <sub>F</sub> = 4.5 eV, field of view of 67 μm), (b) Corresponding work function map within a field of view of 115 μm (Frégnaux, 2016) .....	34
3.17 Illustration of the exfoliation process for HfSe <sub>2</sub> (a) bulk HfSe <sub>2</sub> single crystal, (b) A repeated Scotch tape mechanical exfoliated technique to HfSe <sub>2</sub> thin flakes and (c) A pristine HfSe <sub>2</sub> thin flakes transferred to SiO <sub>2</sub> /Si (p-doped) substrates .....	34
4.1 XPS spectra (dot) and fits (lines) of (a) Hf 4f, (b) Se 3d of the HfSe <sub>2</sub> after 1 day of ambient exposure with 60°, 70°, 80° and 90° take-off angles .....	38
4.2 XPS spectra (dot) and fits (lines) of (a) Hf 4f, (b) Se 3d of the HfSe <sub>2</sub> after 1 day of ambient exposure before and after 1 min, 15 min, and 30 min of Ar ion sputtering .....	40
4.3 PEEM images showing the pristine HfSe <sub>2</sub> thin flakes for the surface oxidation dynamic by H <sub>2</sub> O (a), O <sub>2</sub> (b) exposed in vacuum pressure environment and air (c) and 95±5% RH (d) exposed in atmospheric pressure environment .....	41

## LIST OF FIGURES (Continued)

Figure	Page
4.4 Area probe-XPS spectra of Hf 4f peaks profile by In-situ H <sub>2</sub> O (a), In-situ O <sub>2</sub> (b), Ex-situ air (c) and Ex-situ 95±5% RH (d) exposure in pristine (lower panel), pristine (lower panel), 1 hour exposure (Meddle panel), and 4 hours exposure (upper panel). Dot are experimental data. The 1 <sup>st</sup> and 2 <sup>nd</sup> doublet peaks are corresponding Lorentzian fit to Hf 4f peak for HfSe <sub>2</sub> and HfO <sub>2</sub> respectively.....	43
4.5 Area probe-XPS spectra of Se 3d peaks profile by In-situ H <sub>2</sub> O (a), In-situ O <sub>2</sub> (b), Ex-situ air (c) and Ex-situ 95±5% RH (d) exposure in pristine (lower panel), 1 hour exposure (Meddle panel), and 4 hours exposure (upper panel). Dot are experimental data. The 1 <sup>st</sup> and 2 <sup>nd</sup> doublet peaks are corresponding Lorentzian fit to 3d peak for HfSe <sub>2</sub> and Se-Se bonding respectively.....	44
4.6 PEEM measurements of the HfSe <sub>2</sub> flakes work function mapping for In-situ H <sub>2</sub> O (a), In-situ O <sub>2</sub> (b), Ex-situ 95±5% RH (c) exposure in pristine (upper panel), 1 hour exposure (meddle panel), and 4 hours exposure (lower panel). .....	45



# CHAPTER I

## INTRODUCTION

### 1.1 Background and motivation

Field-Effect Transistors (FETs) used in electronic circuits are made of silicon. Nowadays, Si-based FETs technology has been developed rapidly. Gordon Moore predicted that the number of transistors on integrated circuits will be approximately increased to be double every two years, known as “Moore's law”. This law can be achieved by down-scaling FETs. The large number of down-scaling FETs can be assembled in the circuit leading to the operating at high frequencies. Recently, microprocessors had billions of FETs that can operate the multiple GHz clock speeds for the ability and potential to perform highly complex and fast processing. However, the down-scaling Si-base FETs lead to the short channel effects (SCE) which significantly degrade the device performance. The SCE defines a fundamental limit of scaling.

To reduce the SCE, the research community has begun to investigate alternative channel materials that perform better or give unique functionality to replace Silicon. In 2004, Andre Geim and Konstantin Novoselov synthesized graphene (a single layer of carbon atoms organized in a hexagonal pattern). Graphene has a lot of promising for electrical devices because of its high carrier mobility. However, Graphene is a semiconductor with a zero-band gap ( $E_g$ ) that makes it impossible to stop the movement of electrons. Thus, we cannot create logic-based electron device applications by using graphene. Nevertheless, this discovery could open the way for further research into two-dimensional (2D) materials. Since then, many 2D materials have been discovered such as black phosphorus (BP), Hexagonal-boron nitride (h-BN), MXenes, transition metal dichalcogenides (TMDs).

TMDs, i.e.,  $\text{MoS}_2$ ,  $\text{MoSe}_2$ ,  $\text{MoTe}_2$ ,  $\text{HfS}_2$  and  $\text{HfSe}_2$ , have been the subject of research attention because of their outstanding and unique properties including high on/off current ratio, high carrier mobility, moderate indirect to direct band gap upon

thinning down to monolayer. It suggests their potential in replacing silicon-based semiconductors. Particularly, Hafnium Diselenide ( $\text{HfSe}_2$ ) is the candidate material for the field-effect transistors and metal-insulator-semiconductor owing to very close to silicon band gaps and highest carrier mobility prediction from theoretical study (Zhang et al., 2014). However, the air stability is weak because it can be easily oxidized (Kanazawa et al., 2016; Mirabelli et al., 2016).

Moreover, after being oxidized,  $\text{HfSe}_2$  have a compatible high- $\kappa$  dielectric native oxide of hafnium dioxide ( $\text{HfO}_2$ ). This is advantageous for FET because it can reduce the leakage effect without introducing external mechanical stress on the channel material and the interfacial trap states between the  $\text{HfSe}_2/\text{HfO}_2$  heterostructure, suggesting its advantage for device performance. Normally, most TMD/high- $\kappa$  dielectric gate insulators (for example  $\text{HfO}_2$ ,  $\text{ZrO}_2$ , and  $\text{Al}_2\text{O}_3$ ) cannot be easily integrated (Chhowalla et al., 2013; Azcatl et al., 2014).

In this work, we would like to investigate the oxidation reactivity on  $\text{HfSe}_2$  thin flakes under a range of exposure environments to properly understand the oxidation process of  $\text{HfSe}_2$ . The depth-profiling of oxidized  $\text{HfSe}_2$  surface has also been observed. These are to explore a new avenue to controllable and growth homogenous oxide  $\text{HfSe}_2/\text{HfO}_2$  interfaces.

## 1.2 Research objectives

1.2.1 To study the oxidation reactivity at the surface of  $\text{HfSe}_2$  thin flakes under a range of exposure environments by Photoemission Electron Microscopy (PEEM)

1.2.2 To study the work function variation on the  $\text{HfSe}_2$  surface during the oxidation reaction in each environment exposed by Photoemission Electron Microscopy (PEEM)

1.2.3 To study the depth profiling of oxidized  $\text{HfSe}_2$  by using X-ray Photoelectron Spectroscopy (XPS) that is capable of angle dependent and argon ion sputtering.

### 1.3 Outline of thesis

The thesis is divided into 5 chapters. The chapter I is an introduction to the background and motivation of the limitations of down-scaling Field-Effect Transistors (FETs) and the interesting properties of transition metal dichalcogenides (TMDs). Chapter II presents the literature review. we describe the prototype HfSe<sub>2</sub> based transistor and surface oxidation of HfSe<sub>2</sub> after exposure to air. Chapter III discussed the principle of photoemission, X-ray Photoelectron Spectroscopy (XPS) and Photo Electron Emission Microscopy (PEEM), which are used as a technique for characterization. In chapter IV, we will discuss the HfSe<sub>2</sub> surface after ambient exposure was investigated using an XPS depth profile by nondestructive technique with angle dependent measurement and destructive technique using Argon sputtering. This chapter also discusses the oxidation effects on exfoliated flakes of HfSe<sub>2</sub> under a variety of different exposed condition as well as work function mapping across the flake. Chapter V includes the conclusion and future direction.

## CHAPTER II

### LITERATURE REVIEWS

This chapter provides a summary of the literature review on the issues covered in this thesis. The first part of this chapter describes the prototype HfSe<sub>2</sub> based transistor. The second section includes a discussion of surface oxidation of HfSe<sub>2</sub> after exposure to air.

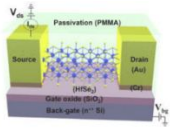
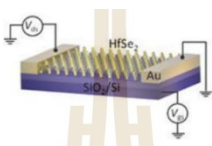
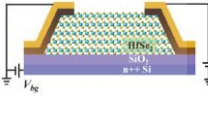
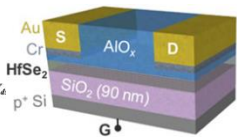
#### 2.1 HfSe<sub>2</sub>-based transistor

According to a theoretical study on TMDs, hafnium diselenide (HfSe<sub>2</sub>) has the highest carrier mobility (Zhang et al., 2014). HfSe<sub>2</sub> has emerged as a potential material for FET. Several groups, such as Kang et al. (2015), Yin et al. (2016), Kang et al. (2017), and Mleczko et al. (2017), have realized and investigated prototype HfSe<sub>2</sub>-based transistors by using conventional oxides grown by Atomic Layer Deposition (ALD) for gate insulators. The specification and performance of each prototype are shown in table 1. The HfSe<sub>2</sub>-based transistor prototype was discovered that a high on/off current ratio, more than 10<sup>6</sup>, could be produced, meeting the requirements for effective switching in digital logic transistors (Kang et al., 2015). But its carrier mobility (0.22 to 4 cm<sup>2</sup>V<sup>-1</sup>s<sup>-1</sup>) is still a significant difference, lower than three orders of magnitude, with a theoretical predicted value (3,500 cm<sup>2</sup>V<sup>-1</sup>s<sup>-1</sup>) at ambient temperature (Zhang et al., 2014). Therefore, to achieve properly operating devices, device optimization in the inclusion of dielectric layers and the selection of appropriate metal contacts should be enhanced.

In this thesis, we are particularly interested in the high-quality interface between the gate dielectric and the channel material because it has a direct influence on the performance. The quality of the dielectric is highly dependent on its preparation procedure. Hence, it is important to choose the most appropriate approach for

this operation. For example, by switching the gate dielectric of a MoS<sub>2</sub> FET from SiO<sub>2</sub> to a high -  $\kappa$  material (HfO<sub>2</sub>), the mobility of MoS<sub>2</sub> can be increased to the theoretical limit (Radisavljevic et al., 2011).

**Table 2.1** The specification and performance of prototype HfSe<sub>2</sub>-base transistors.

	Kang et al. (2015)	Yin et al. (2016)	Kang et al. (2017)	Mleczo et al. (2017)
Schematic diagram				
Interface	SiO <sub>2</sub> / HfSe <sub>2</sub>	SiO <sub>2</sub> / HfSe <sub>2</sub>	SiO <sub>2</sub> / HfSe <sub>2</sub>	SiO <sub>2</sub> / HfSe <sub>2</sub>
Channel	Exfoliated HfSe <sub>2</sub> 17.3 nm (~28 layers)	Exfoliated HfSe <sub>2</sub> ~15.8 nm	Exfoliated HfSe <sub>2</sub> 4.4 to 79.2 nm	Exfoliated HfSe <sub>2</sub> 3 and 13 layers (~1.8 to 8.1 nm)
Channel length (L)	3.6 $\mu$ m	6.8 $\mu$ m	8.2 $\mu$ m	varying from 90 nm to 2.5 $\mu$ m
Channel width (W)	4.4 $\mu$ m	3.6 $\mu$ m	3.6 $\mu$ m	Not report
Electrodes	Cr / Au (10/80 nm)	Au (60 nm)	Cr / Au (10/30 nm)	Cr/Au (15/45 nm)
on/off current ratio	$7.5 \times 10^6$	$10^6$	27 to $10^5$	$\sim 10^6$ at 300 K (approaching $10^7$ for thicker samples cooled to 200 K)
A field effect mobility (cm <sup>2</sup> V <sup>-1</sup> s <sup>-1</sup> )	0.22 (280 K) 0.38 (120 K)	2.6 – 6.5	2.16 to 3.04	1 to 4 (Room temperature)
Condition	In the temperature range of 120 K – 280 K	Room temperature and vacuum condition (10 <sup>-6</sup> Torr)	Room temperature under ambient conditions	Temperature dependence from 80 to 300 K

However, the current approach to the preparation of dielectrics for the HfSe<sub>2</sub>-based transistor is an atomic layer deposition. This method of preparation may be one of the factors contributing to the limitations of FET performance because the previous studies indicate that the formation of island-type dielectrics on a 2D material results in a non-uniform, low-quality dielectric/2D material interface (McDonnell et al., 2013; Xu et al., 2016). Consequently, the performance and practical applicability of 2D material electrical devices are severely limited.

Furthermore, HfSe<sub>2</sub> crystals are not durable for oxidation at ambient conditions, leading to the formation of a HfO<sub>2</sub> layer, meaning that this air sensitive HfSe<sub>2</sub> surface is harmful for transistors. However, HfO<sub>2</sub> is a high- $\kappa$  dielectric oxide that has been frequently applied as a top gate layer for field-effect transistors (Zou et al., 2010; Radisavljevic et al., 2011). Preliminary study by Mleczko et al. (2017) has shown that the use of suitable dielectrics can help decrease interfacial trap states. According to their results, the native HfO<sub>2</sub> layer is capable of successfully suppressing interfacial charge trap states at the HfSe<sub>2</sub>/HfO<sub>2</sub> interface, which is extremely helpful to the device performance. Therefore, understanding the oxidation of HfSe<sub>2</sub> is essential to achieve high-quality native oxide formation in HfSe<sub>2</sub>-based transistors.

## 2.2 The oxidation at surface HfSe<sub>2</sub> after ambient exposure

The optical microscope and AFM were used to investigate the influence of ambient conditions on the stability of HfSe<sub>2</sub> (Kang et al., 2015). The degradation in the surface profile shown in the figures is almost certainly due to surface oxidation. The optical images in Figures 2.1(a) and 2.1(b) illustrate the accelerated degradation of unpassivated-HfSe<sub>2</sub> flakes under ambient conditions after 1 day and 8 days, respectively. They investigated the time-dependent degradation of the exfoliated HfSe<sub>2</sub> flakes using AFM topographic images. The results are presented in Figures 2.1(c) and 2.1(d). The RMS roughness value increases with air exposure time, rising from 2.035 nm after one day to 3.809 nm after eight days in the ambient.

The comparison of surface-sensitive under ambient conditions on the exfoliated flakes of 5 different transition metal dichalcogenides (TMDs) - MoS<sub>2</sub>, MoSe<sub>2</sub>, MoTe<sub>2</sub>, HfS<sub>2</sub>, and HfSe<sub>2</sub> was studied (Gioele Mirabelli et al., 2016). The results showed that MoS<sub>2</sub> and HfSe<sub>2</sub> are the most and least stable after ambient exposure, respectively. Figure 2.2(a) depicts an Atomic Force Microscopy (AFM) image of the HfSe<sub>2</sub> surface taken 24 hours after exfoliation. The several protrusions were observed with approximately 60 nm of height randomly located across the surface. Figure 2.2(b) shows an SEM image of 5 months and 1 - day HfSe<sub>2</sub> surface after exfoliation that appear the same kind of blisters (small protrusions). They chose the 5 - month exposed sample to study the TEM cross-section analysis to demonstrate the obvious image of the blister as shown in Figure 2.2(c). It indicated that HfSe<sub>2</sub> has been modified by localized blisters and planar surface modification after ambient exposure to the surface.

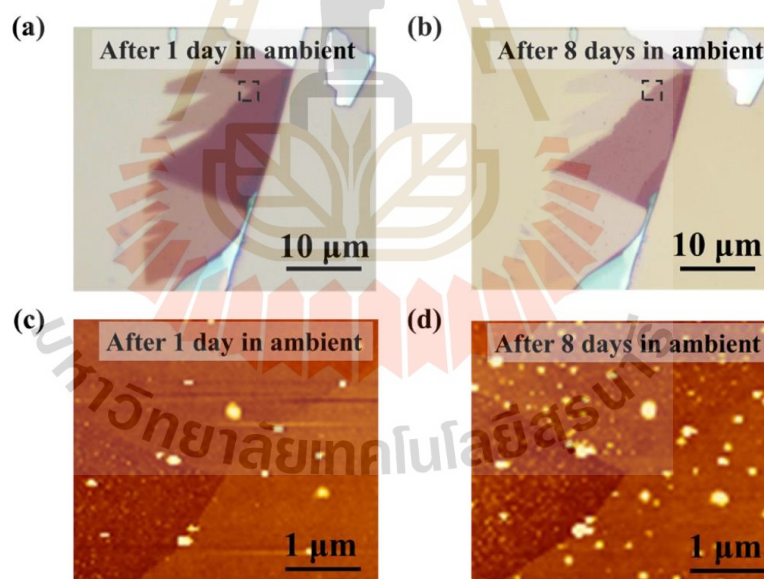


**Figure 2.1** Degradation of exfoliated HfSe<sub>2</sub> flakes over time on a 285 nm SiO<sub>2</sub> substrate. Optical images (a) after 1 day and (b) after 8 days in ambient conditions. The AFM images after 1 day and 8 days in ambient conditions are shown in (c) and (d), respectively. The black dotted boxes in (a) and (b) represent locations where an AFM scanning image was obtained. (Kang et al., 2015)

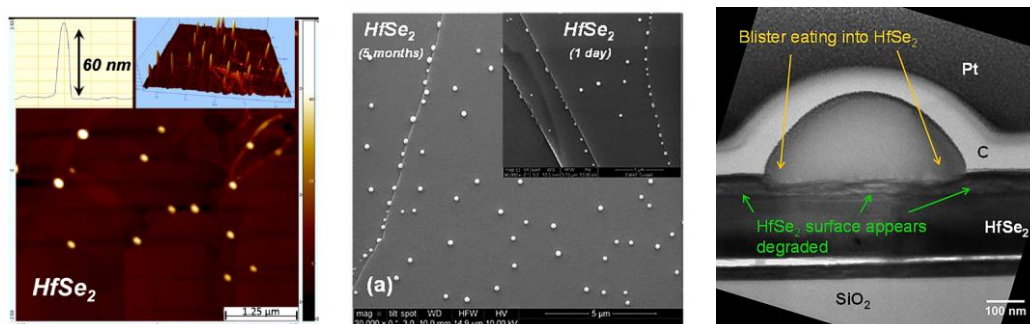


**Figure 2.2** (a) The  $\text{HfSe}_2$  AFM image was taken 24 hours after exfoliation. The cross-section of the tallest protrusion (approximately 60 nm) and a 3D surface feature are shown in the inset. (b) SEM image of  $\text{HfSe}_2$  5 months and 1 day on the inset from exfoliation which shows the same kind of protrusions in terms of form and shape, only smaller. (c) TEM image of the surface blisters on the thick  $\text{HfSe}_2$  flake. (Mirabelli et al., 2016)

The composition analysis on the surface blister was observed by EDX composition mapping analysis. They found that the blister was composed of abundant Selenium whereas Hafnium was the only trace. The  $\text{HfSe}_2$  layer had an increased concentration of Hafnium and Selenium in the same region, which was different from the blister.

The XPS spectrum of the Hf 4f peak is shown in Figure 2.3. The doublet peak of freshly cleaved sample, the peaks of Hf 4f<sub>5/2</sub> and Hf 4f<sub>7/2</sub>, are located at 14.3 eV and 16 eV, respectively (Figure 2.3(a)). They discovered the Hf oxidation component peak at 15.4 and 17.1 eV after continuous exposure to the ambient for 1 hour, 3 hours, and 48 hours. And the intensity of the peaks was increased when the time of exposure was longer, as shown in Figure 2.3(b), (c) and (d). From Figure 2.3(e), the oxide feature can be removed by re-cleaving of the top surface.

The Se 3d peak spectrum is unresolved to doublet peak, the normal peak of Se 3d<sub>5/2</sub> and Se 3d<sub>3/2</sub> are located at 55.4 and 56.4 eV, and there is no significant change after 1 hour, 3 hours, and 48 hours of exposure (Figure 2.4). It indicates that the oxidation of Se is not observed.



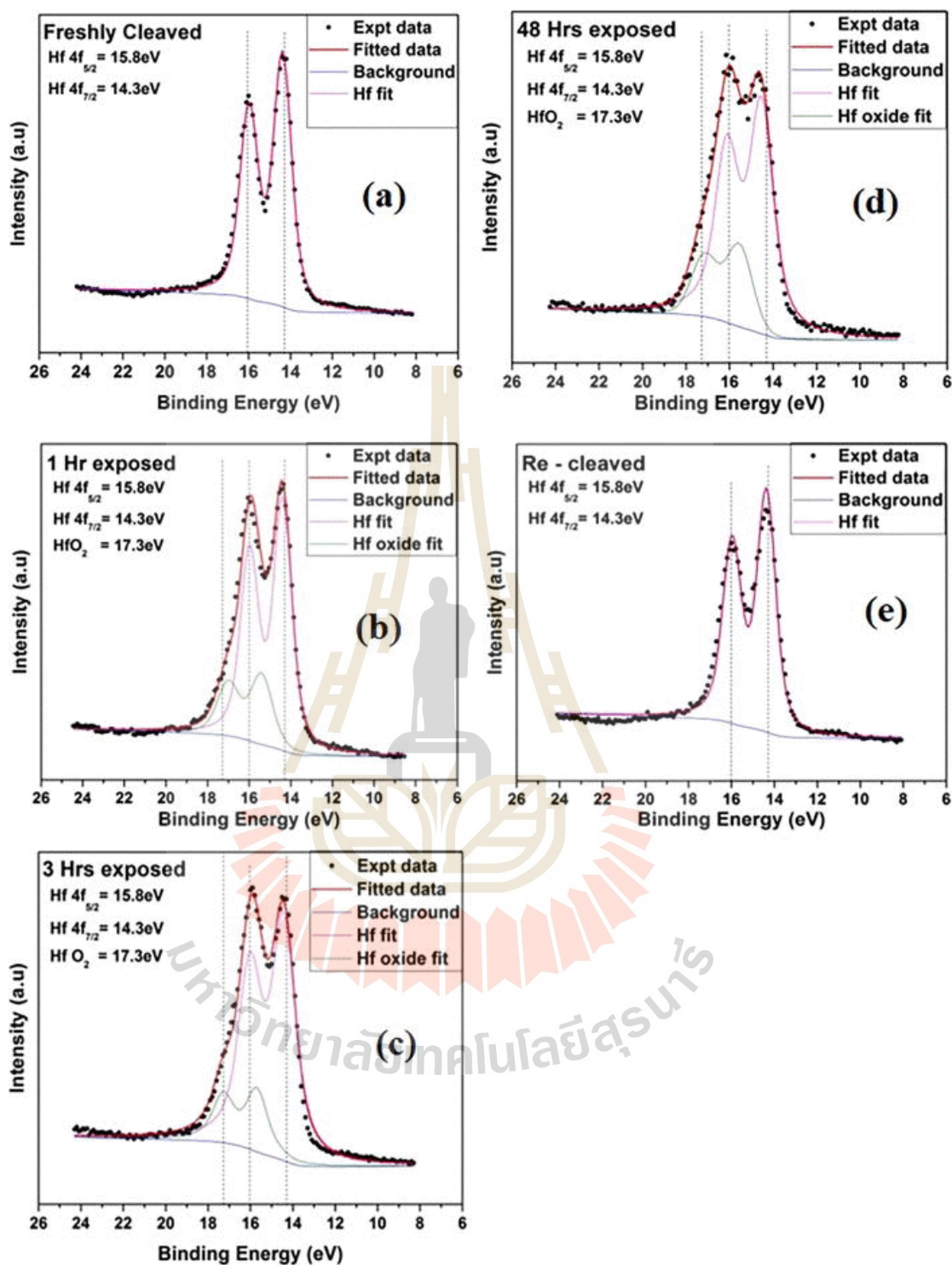


Figure 2.3 Hf 4f peaks XPS spectrum of Hf; freshly cleaved (a), after 1 hour (b), 3 hours (c), and 48 hours (d) ambient exposure and re-cleaving (d). (Gioele Mirabelli et al., 2016)

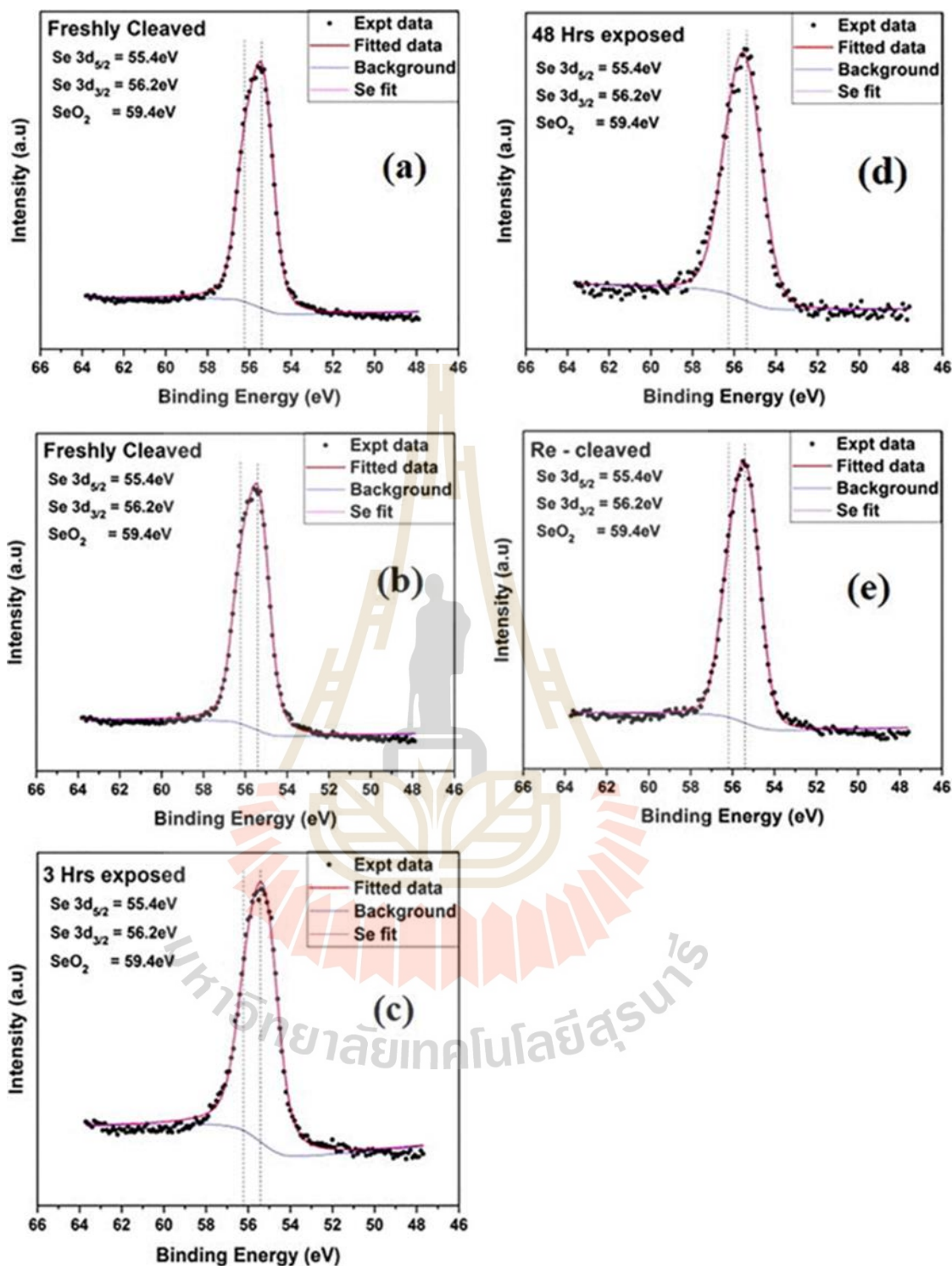
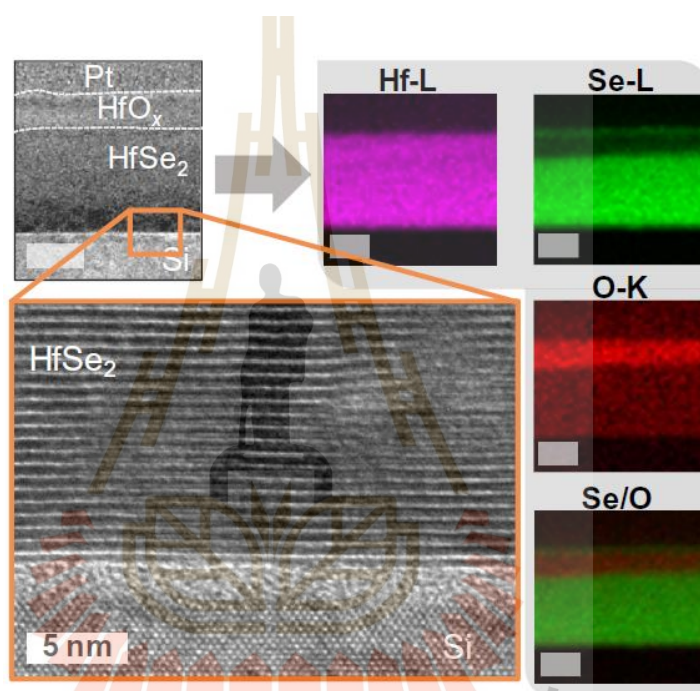


Figure 2.4 Se 3d peaks XPS spectrum of Se; freshly cleaved (a), after 1 hour (b), 3 hours (c), and 48 hours (d) ambient exposure and re-cleaving (d). (Gioele Mirabelli et al., 2016)

To better understand the process of  $\text{HfSe}_2$  oxidation, cross-sectional transmission electron microscopy (TEM) was used for the study (Mleczko et al., 2017). In an inert gas atmosphere [nitrogen glovebox,  $\text{O}_2$  and  $\text{H}_2\text{O} < 1$  part per million (ppm)], multilayer samples were exfoliated onto Si, solvent-cleaned, and exposed to open laboratory air at various time intervals. Figure 2.5 shows a  $\text{HfSe}_2$  flake after seven days of exposure. Despite longer exposure periods creating a thicker amorphous  $\text{HfO}_x$  top film, a pristine bottom interface is obtained against a thin buffer of native  $\text{SiO}_2$ .



**Figure 2.5** Cross-sectional TEM image of  $\text{HfSe}_2$  flake after 7 days of ambient exposure. Insets show EDX elemental mapping revealing complete chalcogen depletion, as seen by the overlap of O and Se signals. The scale bars specify 50 nm. (Mleczko et al., 2017)

These studies show that the ambient oxidation of our layered selenides is not self-limiting because of the oxygen diffusion through atomic-scale defects like Se vacancies. Our large-area, bulk samples estimate initial ambient oxidation rates of 5 to 10 nm per day, depending on the degree of volumetric expansion during this process, and these rates will decrease over time as access is restricted to buried layers. If oxygen and moisture are diffused laterally in thin samples, the oxidation rate will increase.

This rate is further increased by processing in the open air and by heating. It is possible to integrate high -  $\kappa$  dielectrics with these technologically important oxides in innovative ways.

Zafer Mutlu et al. (2018) investigated the air stability of  $\text{HfSe}_2$  single-crystal thin flakes using Raman spectroscopy. Raman characterization was carried out on  $\text{HfSe}_2$  flakes that were taken immediately after exfoliation in air, in a glove box, and after long-term exposure to air, as shown in figure 2.6. The  $A_{1g}$  peak at  $199\text{ cm}^{-1}$  is assigned to  $\text{HfSe}_2$ . Figure 2.6(a) shows that after being exposed to air, the  $\text{HfSe}_2$  shows a broad peak around  $260\text{ cm}^{-1}$ , which is consistent with amorphous Se. In contrast, the amorphous Se peak disappears by exfoliating under the Ar atmosphere in a glove box, as seen in Figure 2.6(b). However,  $\text{HfSe}_2$  flakes after long-term exposure to air have an amorphous Se peak and no  $A_{1g}$  peak in their Raman spectra (Figure 2.6(c)).

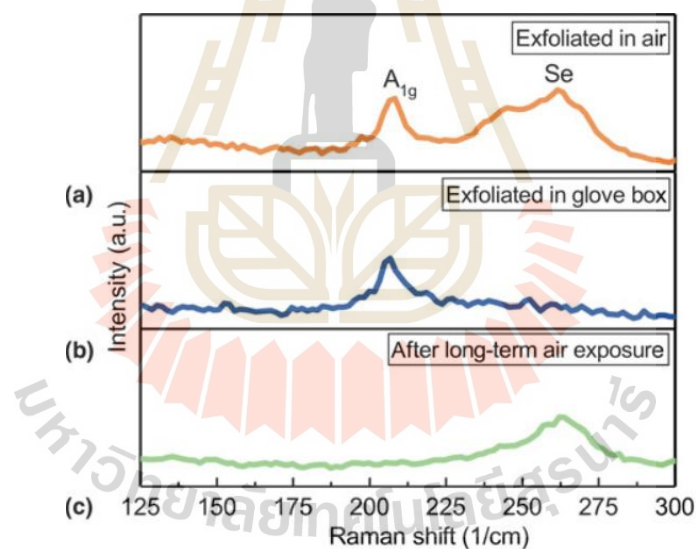


**Figure 2.6** A comparison of the Raman spectra of  $\text{HfSe}_2$  flakes obtained immediately after exfoliation in the air (a), a glove box (b), and after long-term air exposure (c). (Cruz et al., 2018)

Yao et al. (2018) studied the  $\text{HfSe}_2$  surface oxidation dynamics after exposure to air by using scanning tunneling microscopy (STM). The surface topology of the freshly cleaved by mechanical exfoliation is inhomogeneous with a large number of defects

on the surface. The defect density is about  $9 \times 10^{-11} \text{ cm}^{-2}$ , which is higher than  $\text{MoS}_2$  or  $\text{WSe}_2$  (as shown in Figure 2.7). The effect of oxidation on a small  $\text{HfSe}_2$  flake (with a thickness of about 0.74 nm) after air exposure for 2 days was investigated by STM. The  $25 \text{ nm} \times 25 \text{ nm}$  three-dimensional (3D) surface STM topography of the  $\text{HfSe}_2$  surface after 2 days of air exposure shows much rougher than freshly cleaved and finds that oxidized layers have a bandgap of about 2 eV, while the fully oxidized  $\text{HfO}_2$  is about 5.8 eV. It can be indicated that the surface of  $\text{HfSe}_2$  only partially oxidizes and some of the Hf–Se bonds are still preserved.

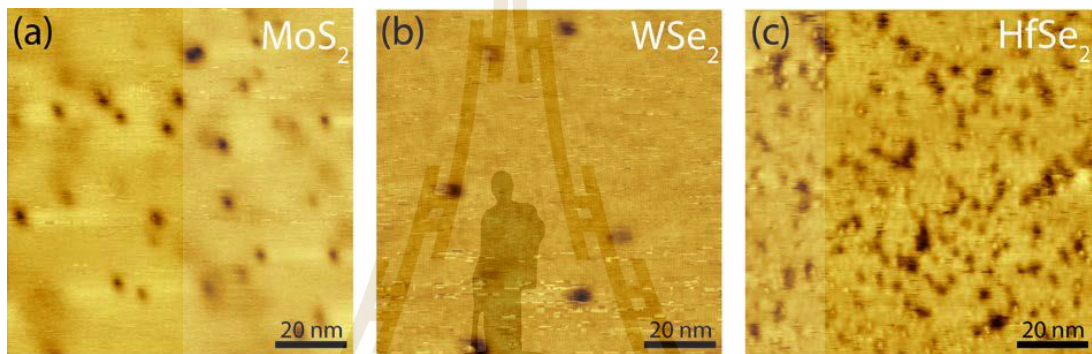


**Figure 2.7** The topography image of  $\text{MoS}_2$ (a),  $\text{WSe}_2$ (b) and  $\text{HfSe}_2$ (c) surfaces, all taken with the same scanning tunneling microscopy conditions. (Yao et al., 2018)

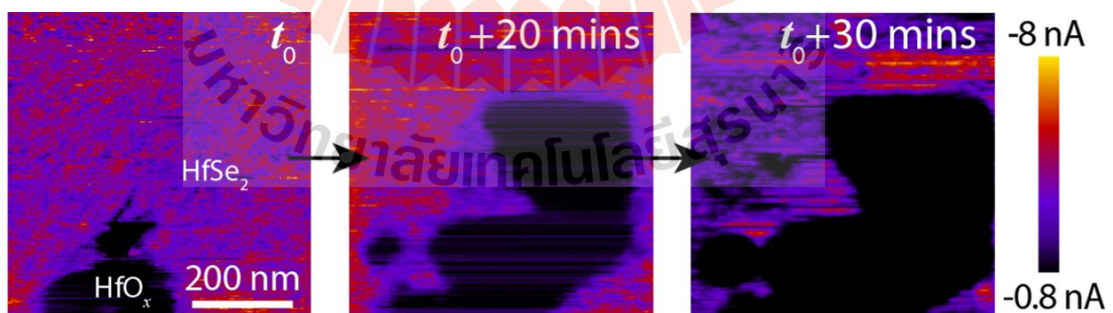


**Figure 2.8**  $\text{HfSe}_2$  oxidation evolution measured with C-AFM at  $t_0$ ,  $t_0+20$  minutes, and  $t_0+3$  minutes. The bias of the sample is 4.7 V. (Yao et al., 2018)

The stability of  $\text{HfSe}_2$  in air exposure was also studied using C-AFM. While the STM experiments used ultrahigh vacuum, the C-AFM experiments used a very low humidity- $\text{N}_2$  atmosphere to exclude the impact of water. However, since the sample is still exposed to oxygen, we can investigate the in-situ oxidation of the topmost  $\text{HfSe}_2$  layers. The  $\text{HfSe}_2$  oxidation process as a function of time is demonstrated in Figure 2.8. At  $t_0$ , the distinct current intensity detected a small oxidized area at the bottom of the frame, which was one order of magnitude lower than that of the pristine surface. You can see that after 20 minutes of scanning the same frame, the oxidized area has spread in all directions, as indicated in the second panel. After 30 minutes, the oxidized area had taken up more than half of the frame.

In this regard, the structural and electrical changes indicate the sensitivity to air of  $\text{HfSe}_2$ . Devices based on  $\text{HfSe}_2$  will require a protective coating layer to avoid oxidation when operating at ambient temperatures. Another method is to use the top layer as a dielectric layer; full oxidation of the uppermost layer prevents the oxidation of the lower layers. As a result, new device designs should be designed to provide for the impacts that have been seen.



## CHAPTER III

### RESEARCH METHODOLOGY

In this chapter of the thesis, we will describe the experiment, which consists of four major sections. The experiment consists of measuring the X-ray Photoelectron Spectroscopy (XPS) depth profile of HfSe<sub>2</sub> flake after ambient exposure and the surface oxidation dynamic under a range of exposure environments by in-situ and ex-situ experiments with Photo Electron Emission Microscopy (PEEM). In the first part, the principle of photoemission will be discussed. The XPS will be clarified in the second part and the third part will describe the PEEM principle. Finally, the experimental procedure will be illustrated in the fourth part.

#### 3.1 Photoemission

Photoemission is a well-known physical phenomenon based on the photoelectric effect, which was discovered by Hertz in 1885 and explained by Einstein in 1905 (Kaja, 2010). When an incoming photon with energy  $h\nu$  is incident on a sample, all electrons with a binding energy ( $E_b$ ) less than  $h\nu$  can change their state from the bound state. If this final state exists for the given excitation energy and the transition is allowed, the obtained energy can remove the electron from the sample, which is called a photoelectron.

In the final state, the excess energy is converted into kinetic energy of the photoelectron. The work function ( $\phi_s$ ) of the material should be considered for the photoelectron that leaves the sample and is detected. The kinetic energy of a photoelectron ( $E_{kin}$ ) is measured from the vacuum level ( $E_{vac}$ ). The Fermi level ( $E_F$ ) for metals is the highest occupied energy level in the solid, which is the important energy level must also be considered. The photoemission principle in solids is demonstrated in Figure 3.1 and the kinetic energy of an emitted photoelectron from the surface is given by

$$E_{\text{kin}} = h\nu - E_b - \phi_s \quad (3.1)$$

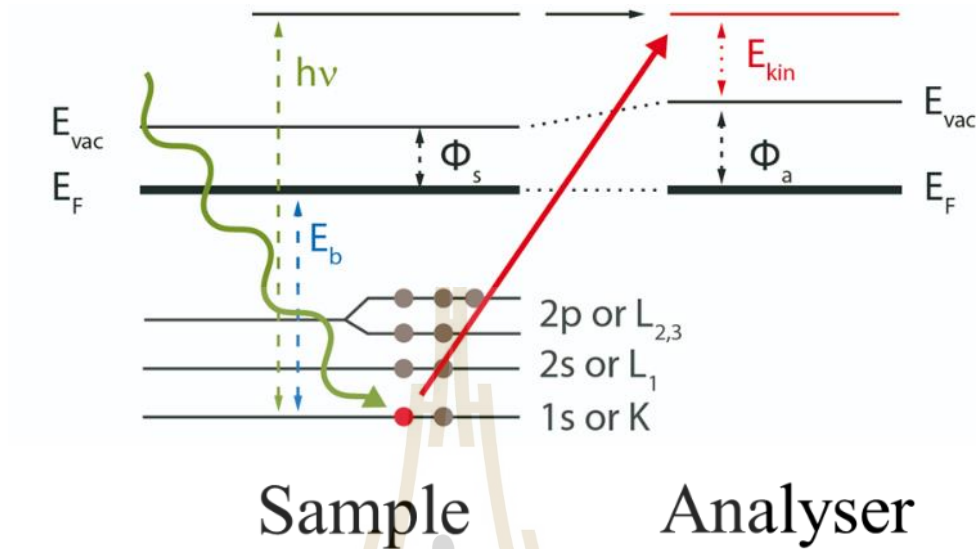


**Figure 3.1** Schematic diagram of the excitation process in Photoemission spectroscopy.

However, the kinetic energy of photoelectrons is measured by the analyzer and the work function of analyzer ( $\phi_a$ ) should be considered. This sample is electrically contacted with the analyzer as demonstrated in Figure 3.1. In the measurement process, the work function, fermi level, and vacuum levels are very to be careful to interpret. The fermi level ( $E_F$ ) of the sample and analyzer are aligned to the same energy which leads to a charge disparity between sample and analyzer that results in a contact potential difference (noted  $eV_s = \phi_a - \phi_s$ ). Hence, the measured kinetic energy of photoelectrons can be expressed by

$$E_{\text{kin}} = h\nu - E_b - eV_s - \phi_s \quad (3.2)$$

From equation (3.2), the total result of the photoelectron's kinetic energy is determined by the work function of the analyzer ( $\phi_a$ ) and it is given by

$$E_{\text{kin}} = h\nu - E_b - \phi_a \quad (3.3)$$



For electrons in solids, they occupy distinct energy levels, which can be either confined energy levels (core levels) or delocalized energy levels (the valence band conduction band of the metals). The core-level binding energy ( $E_b$ ) of the emitting atom is its specific characteristic, depending on the chemical environment (nature of the initial neighbor atoms) and the local atomic environment (length and angles of bonds) in which this atom is located. The binding energy can be calculated from equation (3.3) by measuring the kinetic energy of the emitted photoelectron ( $E_{kin}$ ) from this atom and knowing the work function of the analyzer.

### 3.2 X-ray Photoelectron Spectroscopy (XPS)

The X-ray Photoelectron Spectroscopy (XPS), alternatively referred to as the Electron Spectroscopy for Chemical Analysis (ESCA), was developed by Kai Siegbahn and colleagues as a tool for analytical purposes. Siegbahn was awarded the 1981 Nobel Prize for this work. He proved that it is possible to generate spectra with distinct lines that match to the energy levels of a material. Moreover, He also proved that XPS could be used to determine the chemical composition and local chemical environment of the emitting atom by measuring the binding energy of electrons. As stated in the Koopmans theorem, the initial state of a photoelectron released from a particular atom can may be determined by measuring the amount of energy the photoelectron energy has in its final state (Koopmans, 1934).

Thus, the binding energies of the peaks in an XPS spectrum are distinctive for each element. As demonstrated in Figure 3.2, for the Hf 4f spectrum of air exposure and O<sub>2</sub>-plasma treatment of HfSe<sub>2</sub> flakes, the energy location and peak forms are changed by the chemical state of the emitting atoms. Because of its unique chemical and surface sensitivity, XPS has established itself as a critical and effective tool for surface investigation.

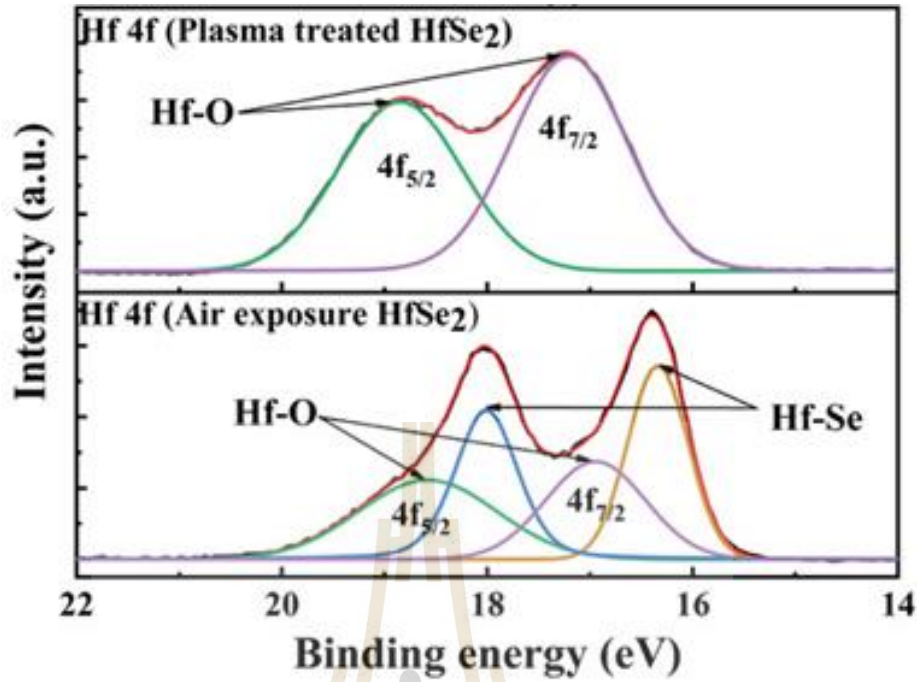


Figure 3.2 Fitted Hf 4f photoelectron spectrum to indicate the chemical state of HfSe<sub>2</sub> flakes after air exposure and O<sub>2</sub>-plasma treatment. (Liu, 2021)

### 3.2.1 Inelastic mean free path

Inelastic mean free path, IMFP or  $\lambda$ , is the average distance that an electron may travel through a material without losing energy due to inelastic scattering. The values of the IMFP of electrons in a material depend on the material structure and kinetic energy of the emitted photoelectrons. With the Tanuma Powell Penn Algorithm (TPP-2M) (Jablonski and Powell, 2022) and the National Institute of Standards and Technology (NIST) database (Powell and Jablonski, 1999), the  $\lambda$  is calculated by equation (3.4).

$$\lambda = \frac{KE}{E_p^2 [\beta \ln(\gamma KE) - (C/E) + (D/E)^2]} \quad (3.4)$$

$$\beta = -0.10 + 0.944(E_p^2 + E_g^2)^{-\frac{1}{2}} + 0.069\rho^{0.1} \quad (3.4a)$$

$$\gamma = 0.191\rho^{-1/2} \quad (3.4b)$$

$$C = 1.97 - 0.91U \quad (3.4c)$$

$$D = 53.4 - 20.8U \quad (3.4d)$$

$$U = (N_v\rho) / M = E_p^2 / 829.4 \quad (3.5e)$$

Where	KE	is the photoelectron energy (in eV)
	$E_p$	is the bulk plasmon energy (in eV)
	$N_v$	is the number of valence electrons per atom (for elemental solid) or molecule (for compounds)
	$\rho$	is the density of the material (in $\text{gcm}^{-3}$ )
	M	is the material atomic or molecular weight

When using conventional XPS, the  $\lambda$  values are generally between 1 and 3.5 nanometers. Thus, the maximum depth is less than 10 nm which can be measured by the XPS technique.

However, photoelectron spectroscopy is very surface sensitive and can only probe the first few atomic layers of a material because of the generally limiting electron mean free path.

### 3.2.2 Sampling depth

Photoelectrons generated with X-rays can move only a limited distance through a solid because of their high inelastic scattering. Photoelectrons emitted from atoms near the surface are unscattered and contribute to the XPS peaks, as illustrated in Figure 3.3, but photoelectrons coming from deeper areas have inelastic collisions with other electrons, which cause them to lose some of their energy.

Only inelastically scattered photoelectrons with enough energy to escape from the sample will contribute to the background (BG) signal at lower KE than the XPS peak. The decrease of initial intensity ( $I_0$ ) of the electron flux released at

a depth  $d$  below the surface can be described by The Lambert-Beer law. As shown in Figure 3.4, the intensity ( $I_d$ ) of the electron flux will drop exponentially with depth when it reaches the surface without scattering, as suggested by Equation (3.5)

$$I_d = I_0 e^{-d/\lambda \sin \alpha} \quad (3.5)$$

where  $\alpha$  is the angle between the electron analyzer acceptance direction and the surface and  $d/\sin \alpha$  is the effective distance travelled through the material. The inelastic mean free path (IMFP), denoted  $\lambda$ , is defined as the average distance that an electron with a given energy travel through a material without inelastic collisions. The probability of an electron escaping at  $\alpha = 90^\circ$  from a depth  $d$  is illustrated in Figure 3.4

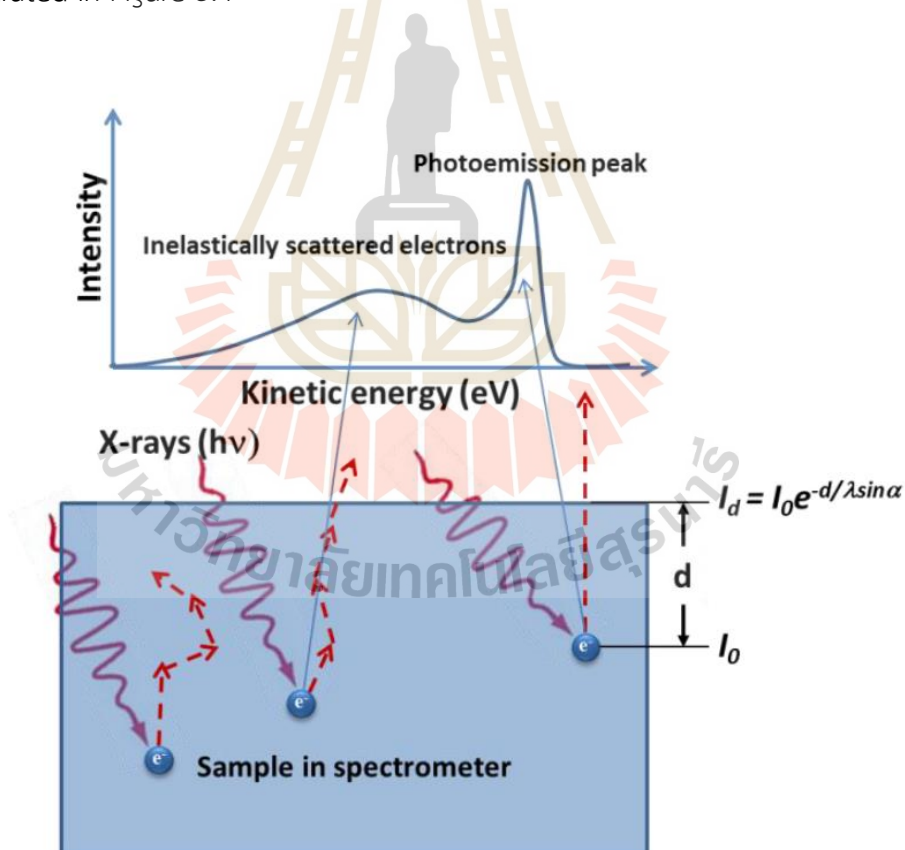


**Figure 3.3** The inelastic scattering process in the sample after it has been irradiation with X-rays results in the formation of a kinetic energy distribution (also known as an electron spectrum). (Sowinska, 2014)

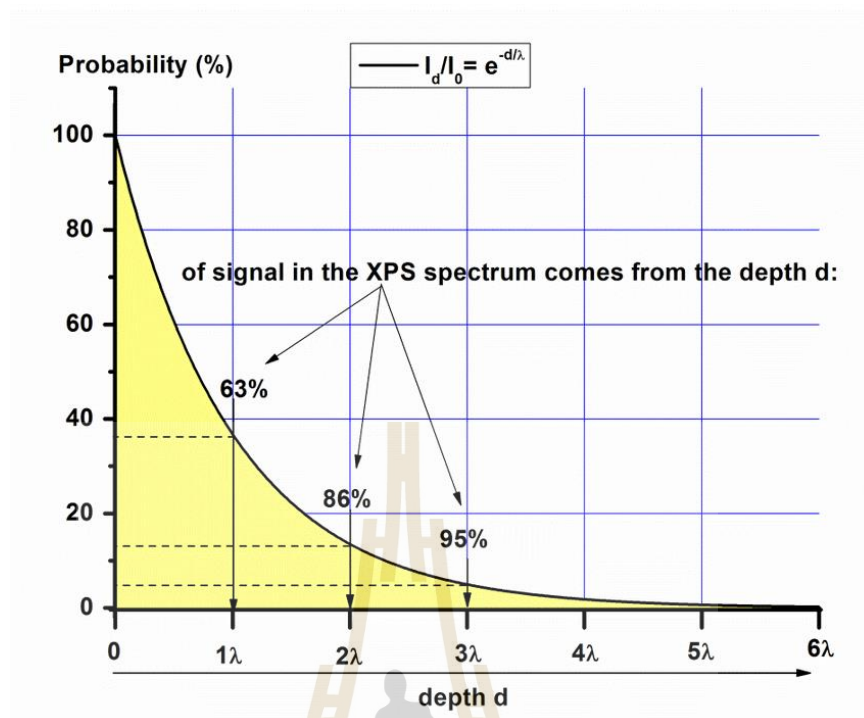


**Figure 3.4** Probability of a photoelectron escaping from a depth  $d$  in normal emission geometry. (Sowinska, 2014)

In the X-ray photoelectron spectrum, it can be observed that about 63% of the signal will emerge from a depth less than  $\lambda$  whereas a depth of less than  $2\lambda$  and  $3\lambda$  can be observed 86%, and 95% of signal, respectively. Thus, the information depth (ID) of the XPS experiment is defined as the depth from which 95% of all photoelectrons which are released by the time that they reach the surface, as suggested by Equation (3.6)

$$d = 3\lambda = \text{ID} \quad (3.6)$$

However, if the  $\alpha$  is less than 90 degrees ( $\alpha < 90^\circ$ ), the measured vertical depth will reduce by a factor of  $\sin \alpha$

$$\text{ID}_\alpha = 3\lambda \sin \alpha \quad (3.7)$$

### 3.2.3 XPS depth profiling

From the XPS information depth (ID) depends on  $\lambda$  and  $\alpha$ , it is possible to investigate the chemical composition as a function of depth. This section will be presented the XPS depth profiling technique. This approach is used to identify the depth distribution of elements that are deeply buried in a material by using nondestructive and/or destructive methods.

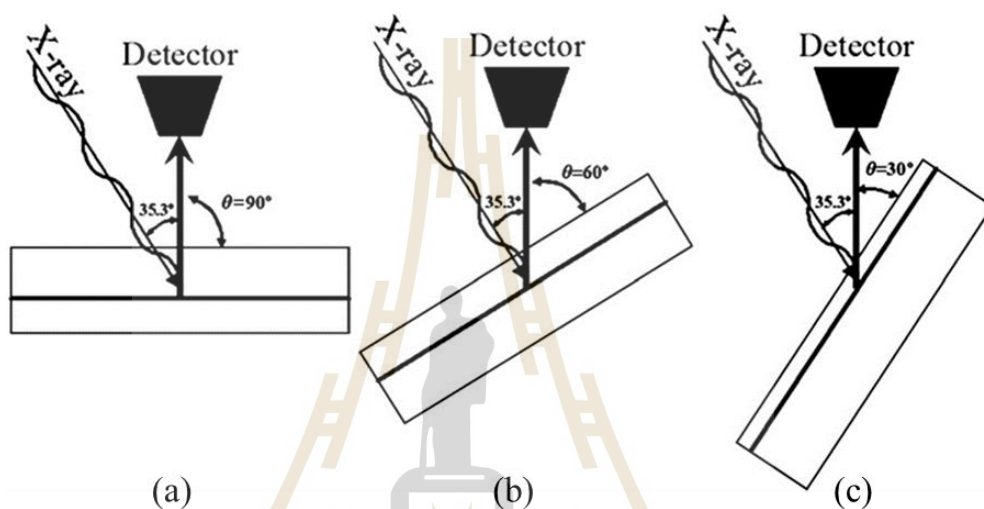


**Figure 3.5** The conventional (a) and angle dependent XPS at  $\alpha = 60^\circ$  (b),  $\alpha = 30^\circ$  (c) experimental setup. (Schneider et al., 2005)

#### 3.2.3.1 Angle Dependents XPS depth profiling

Angle Dependent X-Ray Photoelectron Spectroscopy is a common technique for nondestructive depth profiling using XPS that use to detect the distribution of elements in a material without destroying the sample. Figure 3.5. shows a schematic of the experimental setup for Angle Dependent X-Ray Photoelectron Spectroscopy. The excitation energy is fixed in this approach, whereas the  $\alpha$  is adjusted. It is obvious that the change  $\alpha$  is directly related to ID.

### 3.2.3.1 XPS sputtering depth profiling

This section will discuss the XPS sputtering depth profiling technique (Figure 3.6). This approach is used to establish the distribution of elements buried deeply inside a material. Sputtering depth profiling with XPS is generally performed with an ion sputtering on the sample using Ar, Xe, and other ions, this is a destructive characterization approach. The approach use producing ions with appropriate kinetic energy to remove the surface atoms of the sample. A depth profile can be obtained if a sample surface is evenly cleaned by ion sputtering.

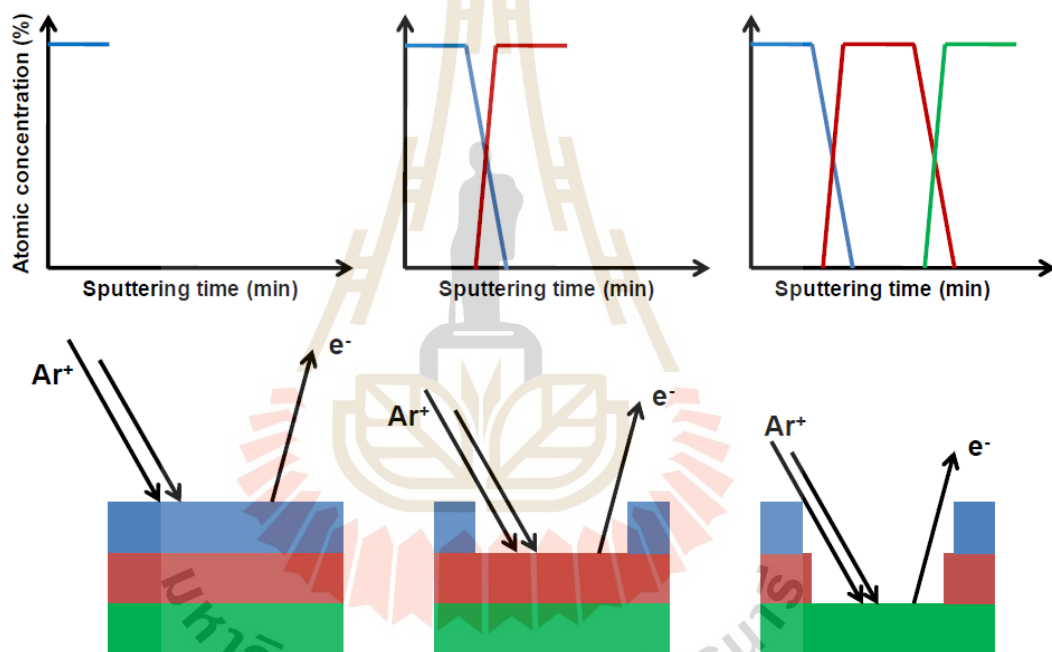


Figure 3.6 Schematic of the XPS sputtering depth profiling method. (Zborowski, 2018)

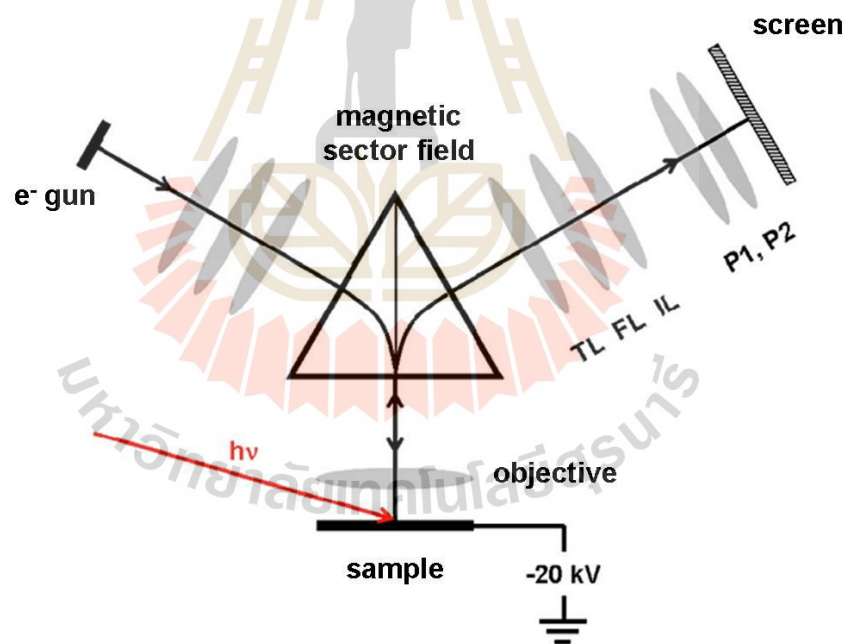
## 3.3 Photo Electron Emission Microscopy (PEEM)

Photo electron emission microscopy (PEEM) can create an image of a surface by combining the photoelectric effect with spatial photothreshold variations. The PEEM technique has a surface sensitivity because the photoelectrons utilized to produce the image come from electronic states near the surface of the material.

In the early 1930s, Bruche invented the photoelectron emission microscope. Bruche imaged a zinc sample target on a fluorescent screen using electrons produced

from the target during UV irradiation. Bruche's microscope had a modest magnifying power and was capable of imaging fields of view (FoV) in the millimeter range. It is also feasible to illuminate the sample surface with a low-energy electron beam and record pictures of the reflected electrons. This technique is referred to as Low-Energy Electron Microscopy (LEEM).

Following Bruche's pioneering work and Recknagel's theoretical work, Spivak et al., Berthge et al., and Mollensted et al. refined and enhanced the approach. PEEM's first commercial version was created in the 1960's. Teliyps and Bauer made a significant development when they created a LEEM picture using a sophisticated electron-optical system and ultrahigh vacuum (UHV). The atomic terraces of a Mo(110) surface could be seen. According to the measurements made by Teliyps and Bauer, the imaging scale was on the order of the micron.



**Figure 3.7** The PEEM technique's operating principle.

Figure 3.7 represents a schematic view of the PEEM technique's operating principle. The sample is irradiated with light (UV-lamp or synchrotron X-rays), and the emitted photoelectrons from the surface are utilized for imaging. A high voltage,



generally between 10 and 20 kV, enables an extraction lens to gather photoelectric emissions from a wide variety of emission angles. After that, a set of lenses focuses and produces a first intermediate picture. Finally, the magnification of this initial picture is accomplished by a set of projection lenses. The detector is composed of a multichannel plate connected to a fluorescent screen and photographed by a CCD camera. Furthermore, the addition of a magnetic sector field to the system is able to execute LEEM on the same sample surface.

A PEEM image is generated by collecting the energy distributions of all the electrons released from the sample surface following photon irradiation. The contrast mechanism for PEEM is caused by variations in surface photoelectron yield and topographically related field enhancement (Wegmann, 1972). The photoelectron yield, denoted by  $Y$ , is defined as the number of released electrons per photon that is incident on the sample

$$Y = \frac{\text{\# of photoemitted electrons}}{\text{\# of incident photons}} \quad (3.8)$$

and the photoelectron yield increases proportional to (Pankove, 1975)

$$Y = A (h\nu - E_{th})^r \quad (3.9)$$

where

- $A$  is a constant
- $h\nu$  is the photon energy
- $E_{th}$  is the photothreshold
- $r$  is a material dependent parameter

The photothreshold is defined as the minimum photon energy required to detect electron emission. For example, the photothreshold of a metal is the same as the surface work function of the metal. For a semiconductor, the photothreshold is related to the band gap energy ( $E_g$ ) and the electron affinity ( $\chi$ ) of the material.

Excitation, surface states, defects, and doping levels are all reasons for emission which occur from semiconductors.

The basic contrast mechanism in PEEM is formed by spatial changes in photoelectron yield. When a surface contains materials or areas with different photothresholds, the photon energy of the incoming photons can be chosen in such a way that the maximum contrast is produced between the materials or regions.

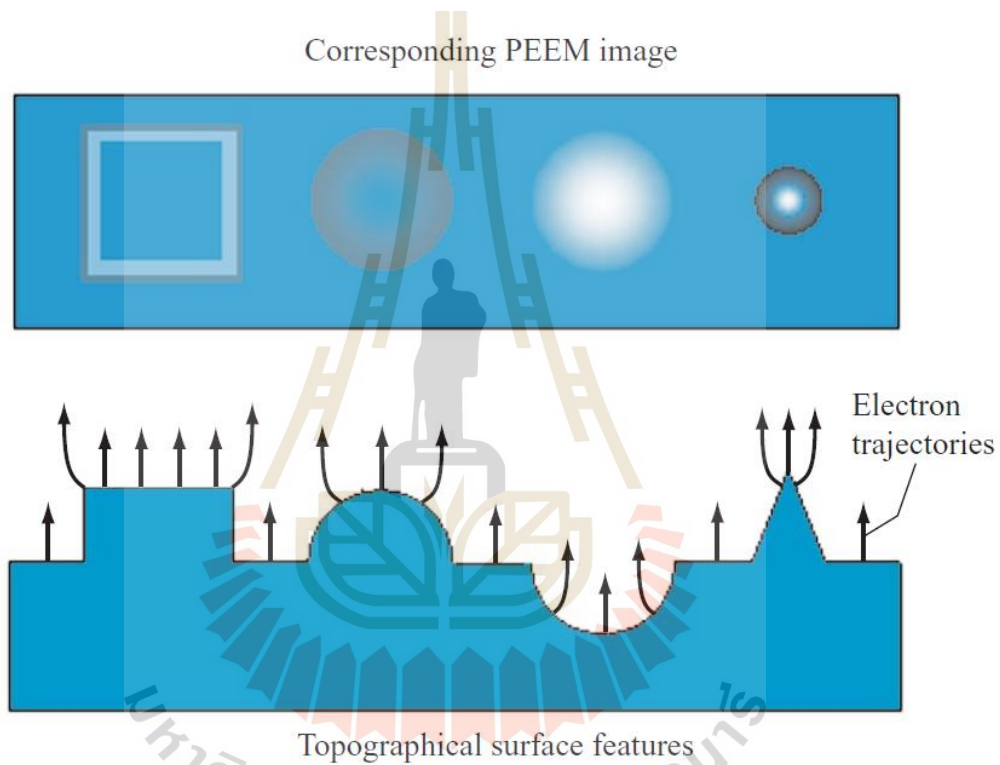


**Figure 3.8** The surface features of the topography and their related PEEM image. (Stohr and Anders, 2000)

Topographic contrast is another important PEEM contrast mechanism, which is related to the effect of surface relief on the electric field. The topological contrast is seen on rough samples and is generated by the electric field being distorted around the surface's topography features. The electron trajectory is disrupted by the distortions in the field distribution, resulting in image contrast. The surface topography and corresponding PEEM images are represented in Figure 3.8.

### 3.3.1 X - ray photo electron emission spectromicroscopy (XPEEM)

The XPEEM combines Photoemission spectroscopy (PES) (also known as photoelectron spectroscopy and XPS stands for X-ray Photoelectron Spectroscopy) with Photoemission Electron Microscopy (PEEM). XPEEM gives access to the electrical and chemical structure of surfaces with spatial resolutions ranging from hundreds to tens of nanometers. This is very useful for surface studies because nanometer-sized interested areas of the sample can be obtained.

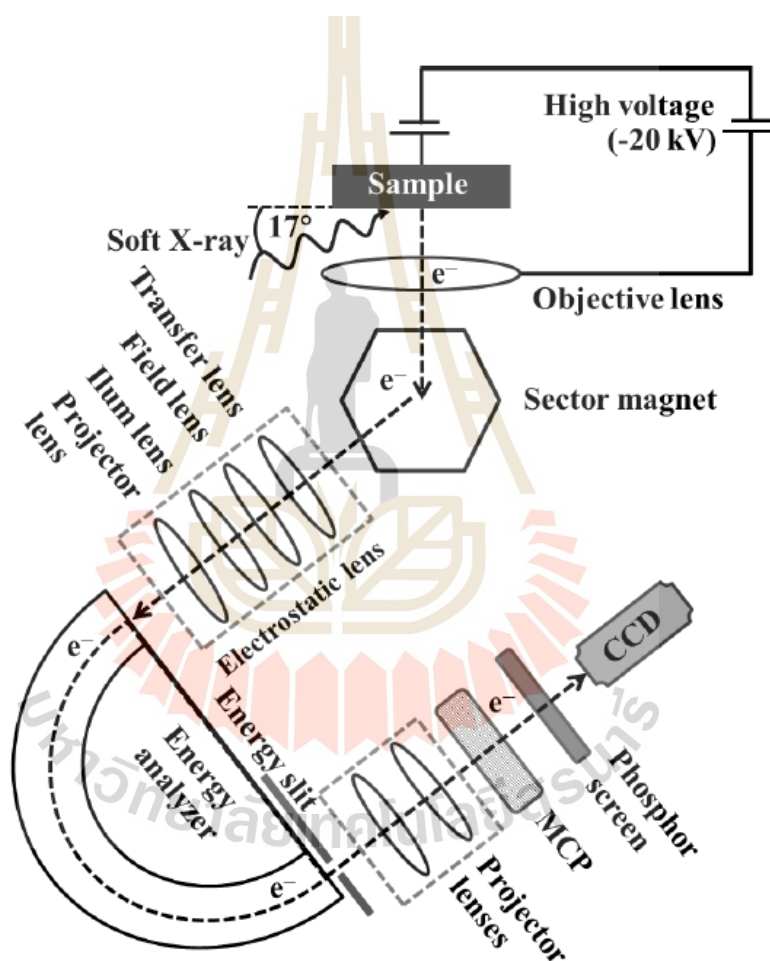


**Figure 3.9** A schematic view of the XPEEM. The instrument is performed at the BL3.2Ub in the Synchrotron Light Research Institute (SLRI), Thailand. (Tunmee, 2016)

For XPEEM spectromicroscopy, a unique technique involves integrating an energy filtering analysis (using a hemispherical energy analyzer) to a PEEM with complete electrostatic lenses, show in Figure 3.9. When electrons are photo-ejected from a surface, they leave with a distribution of kinetic energies. If operating in the energy filtered imaging mode, the XPEEM will be selected the region of the photoelectron spectrum to be image (selected energy windows, as illustrated in figure 3.10). This demonstrates that XPEEM spectromicroscopy is used to study the whole photoelectron spectrum in the sample.

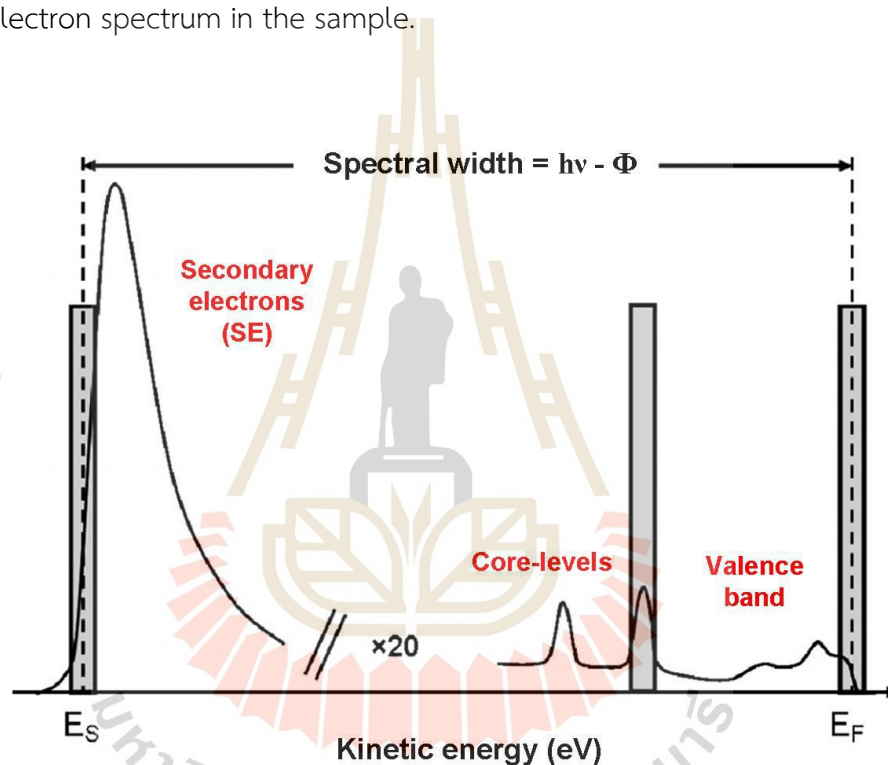


**Figure 3.10** A schematic of a photoelectron spectrum displaying the wide range of kinetic energies that may be selected. (Barrett and Renault, 2009)

From figure 3.10, we can image the photoemission threshold area (using an energy window in the secondary electron range). This provides direct access to work function lateral variations.

Figure 3.11 shows the contrast process that arises in XPEEM imaging mode. The upper circles are XPEEM image of a material 1 that is placed on a material 2.

Differential photoemission spectra of the two materials can be observed. The work function of material 1 is greater than that of material 2. The photoemission peak represented by x is unique to material 2, the peak identified by y is unique to material 1, and the peak denoted by z is common to both materials. The total photoelectron yield image in Figure 3.6(a), which means that all the kinetic energy is being collected. The PEEM image in this case reveals a slight contrast between them because the work functions are differences between two materials. Figure 3.11(b) and (c) represent energy filter image. The kinetic energy window shown in Figure 3.11(b) contains the photoemission peak x. It looks significantly brighter in the XPEEM image because the photoemission peak x is unique to material 1. However, the XPEEM image in Figure 3.11(c) shows no contrast because the energy window encompasses the photoemission peak z, which is common to both materials.

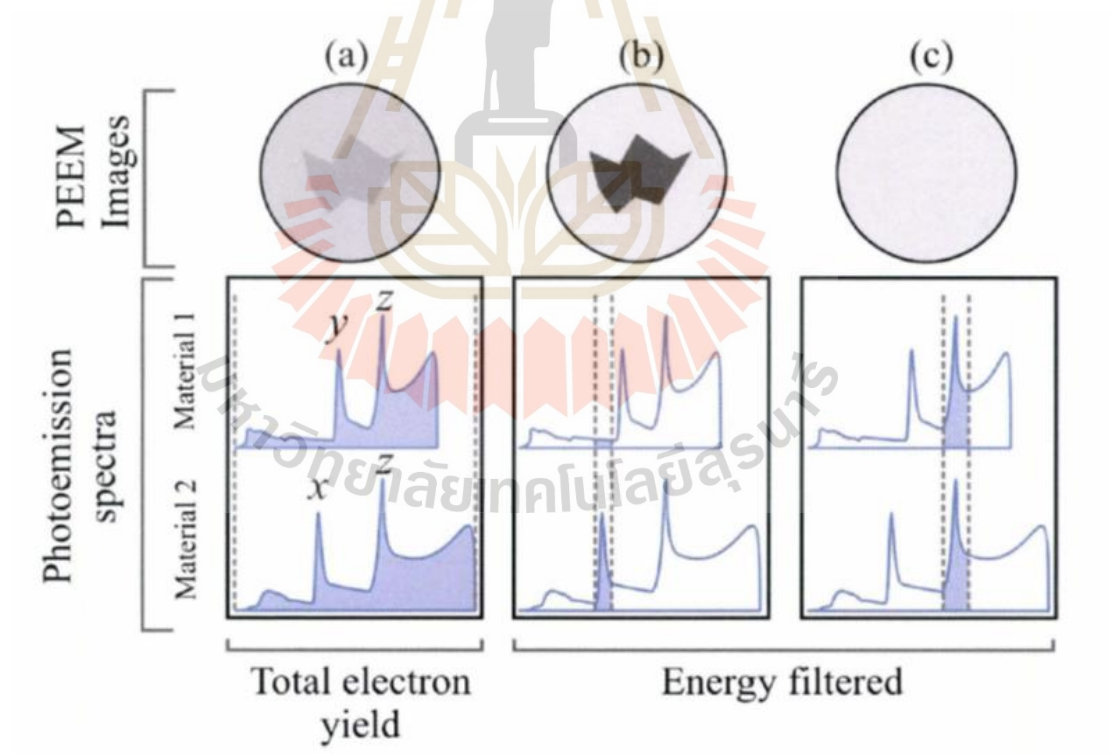


**Figure 3.11** In the XPEEM imaging mode, the contrast is obtained by utilizing (a) total photoelectron yield and (b) and (c) the energy filter, respectively. (Greiner, 2007)

### 3.3.2 Area probe X-ray Photoelectron Spectroscopy (Area probe-XPS)

Area probe-XPS works on the same principles as XPS, which are explained in Section 3.2. A constant photon energy is utilized to probe the surface as well as the emitted electrons are analyzed by using a band pass filter. Instead of just detecting electrons, the final two lenses are used to project the dispersive plane from the energy analyzer onto the detector. This is represented as a horizontal line, where the position along the line represents the binding energy along the observed spectrum and the intensity represents the number of counts. Line profiles is the collecting spectrum of intensity and binding energy, which is similar to XPS, but the energy range is determined by a dispersive plane in Area probe-XPS. For example, the dispersive plane is used to create XPS spectra of Si 1s and Ag 3d photoelectrons as shown in figure 3.12(a) and figure 3.12(b), respectively. By placing Field Limiting Apertures (FLA) on the picture plane in the middle of the beam separator, the probed area can be as small as  $2 \mu\text{m}$ .

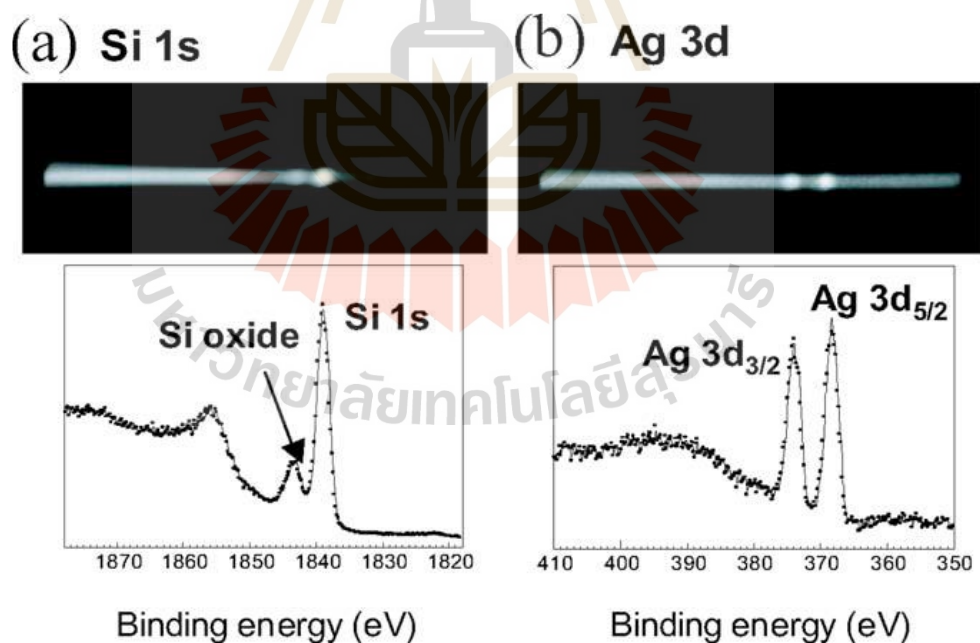


**Figure 3.12** (a) Si 1s and (b) Ag 3d photoelectron energy dispersion spectral images and their intensity plot profiles. (Yasufuku et al., 2006)

In comparison to XPS, Area probe-XPS has a quicker acquisition time with an appropriate signal to noise ratio, which is a major advantage. For example, the Sn  $3d_{5/2}$  core level Area probe-XPS spectrum on electro-deposited gold-tin patterns ( $100\ \mu\text{m} \times 20\ \mu\text{m}$ ) was shown in Figure 3.13. The Area probe-XPS spectrum was measured in two regions which are the region over the whole field of view (blue rectangle) and the region on the pattern by reducing the PEEM column's iris aperture to about  $20\ \mu\text{m}$  (red rectangle) as shown in the XPEEM image inset.

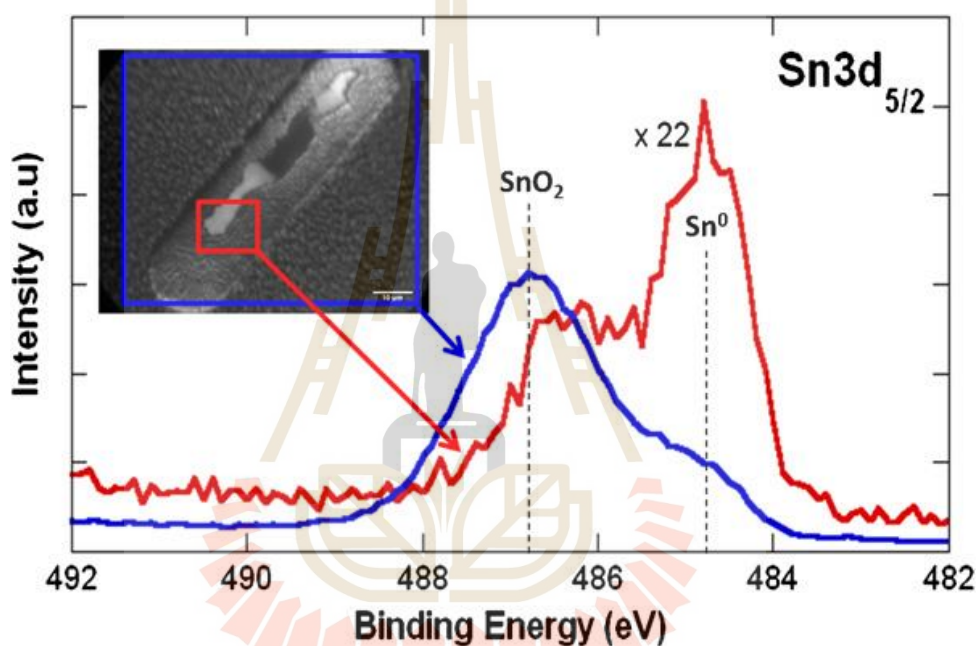


**Figure 3.13** Area probe-XPS spectra of Sn  $3d_{5/2}$  obtained throughout the whole field of vision (blue) and on the pattern using a  $20\ \mu\text{m}$  iris aperture (red). (Renault et al., 2012)

### 3.3.3 Work function measurement and mapping

We show how the local work function is calculated when the surface is scanned using the energy-filtered mode in the secondary electron range (emission threshold range).

Figure 3.14 illustrates a method for determining the work function of materials using photoelectron spectra. As a result of this, the cut-off energy must be determined at both low and high binding energies. In general, biasing the sample is

required to avoid effects caused by the instrument's work function and push all secondary electron out from the surface of solids. The following relationship can be used to calculate the work function of the sample:

$$\phi_s = h\nu - E_{\text{cutoff}} - E_F \quad (3.10)$$

Where  $h\nu$  is the photon energy of the excitation  
 $E_F$  is the Fermi energy level and  
 $E_{\text{cutoff}}$  is low kinetic energy cutoff

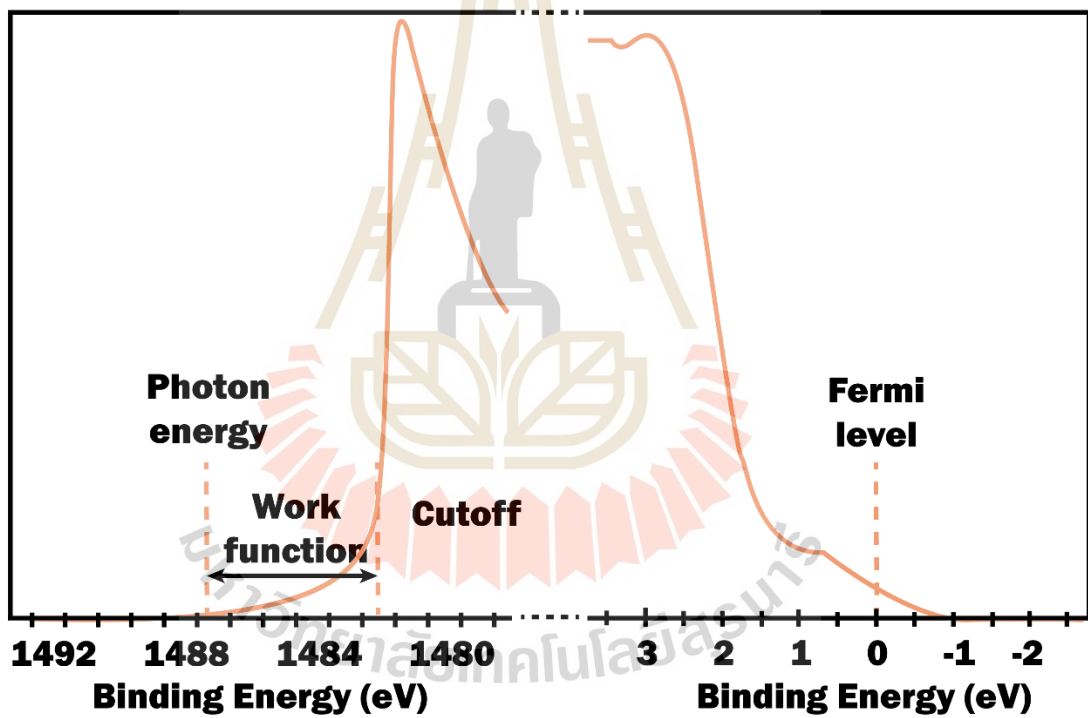
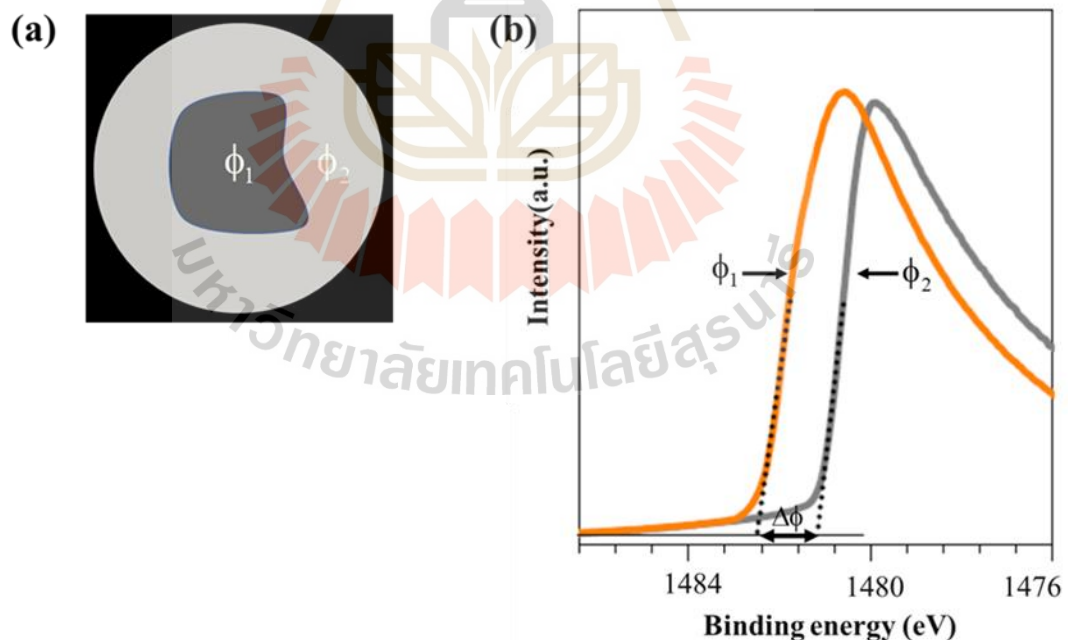


Figure 3.14 A part of the gold survey spectrum obtained with monochromatic Al K- $\alpha$  radiation. (Azo materials, 2020)



The Fermi level ( $E_F$ ) of a semiconductor sample may be measured using the photoelectron spectra of a metal. Normally, when a sample is electrically connected to gold, the Fermi edge is utilized to determine  $E_F$ .

In this work, we measure relative work function mapping by photoemission electron microscopy (PEEM) to obtain spectra with a position-space resolution. The present method reveals an idealized emitter surface with work function patches that are illustrated in Figure 3.15. In this manner, the work function variation of an inhomogeneous surface can be detected relative to any fixed reference value through measurement of the distinct cutoffs for the secondary electron spectra. The work function map is reproduced from the values obtained at each image pixel, such as Frégnaux (2016) shows in the case of a  $\text{MoS}_2$  1L domain transferred onto an Au substrate. Complementary error functions were employed in an energy filtered PEEM image (Figure 3.16 (a)) series to fit the energy-dependent intensity curve for each pixel in order to get the local work function value, as shown in Figure 3.16(b).



**Figure 3.15** Principle of work function mapping.

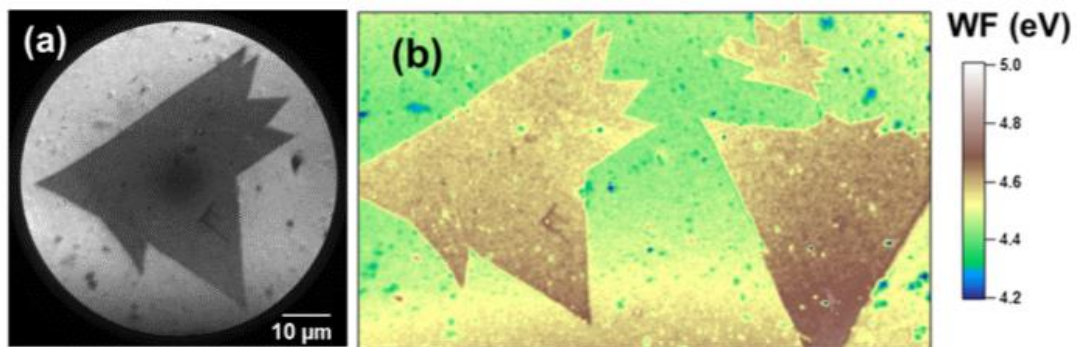


**Figure 3.16** (a) Energy filtered PEEM image ( $E-E_F = 4.5$  eV, field of view of  $67 \mu\text{m}$ ), (b) Corresponding work function map within a field of view of  $115 \mu\text{m}$ . (Frégnaux, 2016)

### 3.4 Experimental Procedure

#### 3.4.1 Sample preparation

We prepared thin flakes that were purchased from HQ graphene Co., Ltd by mechanical exfoliation from a bulk crystal (Figure 3.17(a)). HfSe<sub>2</sub> small pieces were spread on the scotch tape as shown in Figure 3.17(b).

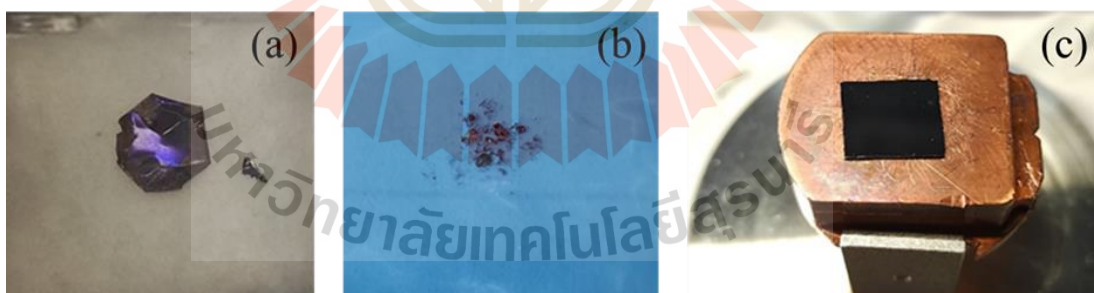


**Figure 3.17** Illustration of the exfoliation process for HfSe<sub>2</sub> (a) bulk HfSe<sub>2</sub> crystal single crystal, (b) A repeated Scotch tape mechanical exfoliated technique to HfSe<sub>2</sub> thin flakes and (c) A pristine HfSe<sub>2</sub> thin flakes transferred to SiO<sub>2</sub>/Si(p-doped) substrates.

To reduce its layer thickness, we cleaved several times to obtain pristine HfSe<sub>2</sub> thin flakes and then transferred them to the SiO<sub>2</sub>/Si(p-doped) substrate (Figure 3.17(c)). These exfoliated materials would later be loaded into the load-lock vacuum chamber (5x10<sup>-6</sup> Pa) to avoid atmospheric contamination.

### **3.4.2 The oxidation reaction at surface of Hafnium diselenide (HfSe<sub>2</sub>) in vacuum pressure environment**

In this study, we investigated the surface oxidation of HfSe<sub>2</sub> by dosing H<sub>2</sub>O and O<sub>2</sub> into the preparation chamber (2x10<sup>-6</sup> Pa), a particularly designed system located at Beamline 3.2b, Synchrotron Light Research Institute (Public Organization) (SLRI), Thailand. Dosage of the H<sub>2</sub>O and O<sub>2</sub> were performed at room temperature with ultra-deionized (DI) water vapor and ultrapure oxygen gas respectively at 4.5x10<sup>-2</sup> Pa pressure.

### **3.4.3 The oxidation reaction at surface of Hafnium diselenide (HfSe<sub>2</sub>) in atmospheric pressure environment**

In this study, we investigated the surface oxidation of HfSe<sub>2</sub> by air and 95±5% relative humidity (RH) exposure in an atmospheric pressure environment. The air was applied to the HfSe<sub>2</sub> thin flakes in a beaker; we then sealed it with aluminum foil. The 95±5% RH condition was then applied by putting the samples in a sealed beaker with DI water heated to 50°C.

### **3.4.4 Sample characterization**

The chemical state compositional information of oxidized HfSe<sub>2</sub> thin flakes will be investigated using depth profiling techniques using XPS in angle dependent and argon ion sputtering mode.

The microscopic study of pristine HfSe<sub>2</sub> thin flakes was investigated by photoemission electron microscopy (PEEM). The variation of oxidation reactivity at the surface of HfSe<sub>2</sub> was performed by the chemical state analysis using Area probe-XPS during exposure times of 1 hour and 4 hours, respectively, and work function variation

measurements over the surface were also observed by mapping. We use In-situ studies for H<sub>2</sub>O and O<sub>2</sub> exposure in a vacuum pressure environment and Ex-situ studies for air and 95±5% RH exposure in an atmospheric pressure environment.



## CHAPTER IV

### RESULTS AND DISCUSSION

The results and discussion of this work will be presented in this chapter. We will start with the XPS depth profile of the HfSe<sub>2</sub> surface after ambient exposure by nondestructive technique with angle dependent measurement and destructive technique using Argon sputtering. The results of oxidation effects on exfoliated flakes of HfSe<sub>2</sub> under a range of various exposure conditions, as well as work function mapping throughout the flake for PEEM measurement, are shown in this chapter.

#### 4.1 The depth profile of Hafnium Diselenide (HfSe<sub>2</sub>) surface after ambient exposure

To determine the chemical state of elements on the HfSe<sub>2</sub> flake after 1 day of ambient exposure, the XPS spectra of all elements are recorded and deconvoluted using a mix of Gaussian and Lorentzian fits.

##### 4.1.1 Angle-dependent XPS depth profile

The HfSe<sub>2</sub> surface after ambient exposure was investigated using an angle dependent XPS depth profile. For each chemical state, the electron binding energy was used to determine its position in high resolution scan of Hafnium (Hf) 4f and Selenide (Se) 3d. These experiments comprised four take-off angles of 60°, 70°, 80° and 90°.

The first experiment investigation for the ambient exposure HfSe<sub>2</sub> was done at 60° for the upper sampling depth. Figure 4.1(a) shows that the Hf-Se (1<sup>st</sup> doublet peak) and Hf-O (2<sup>nd</sup> doublet peak) species contributed to the deconvolution of the Hf 4f photoelectron spectra for ambient exposure HfSe<sub>2</sub>, with binding energies positions of Hf 4f<sub>5/2</sub> at ~18.79 eV and Hf 4f<sub>7/2</sub> at ~17.08 eV for 1<sup>st</sup> doublet peak and Hf 4f<sub>5/2</sub> at ~20.17 and Hf 4f<sub>7/2</sub> at ~18.37 eV for 2<sup>nd</sup> doublet peak.

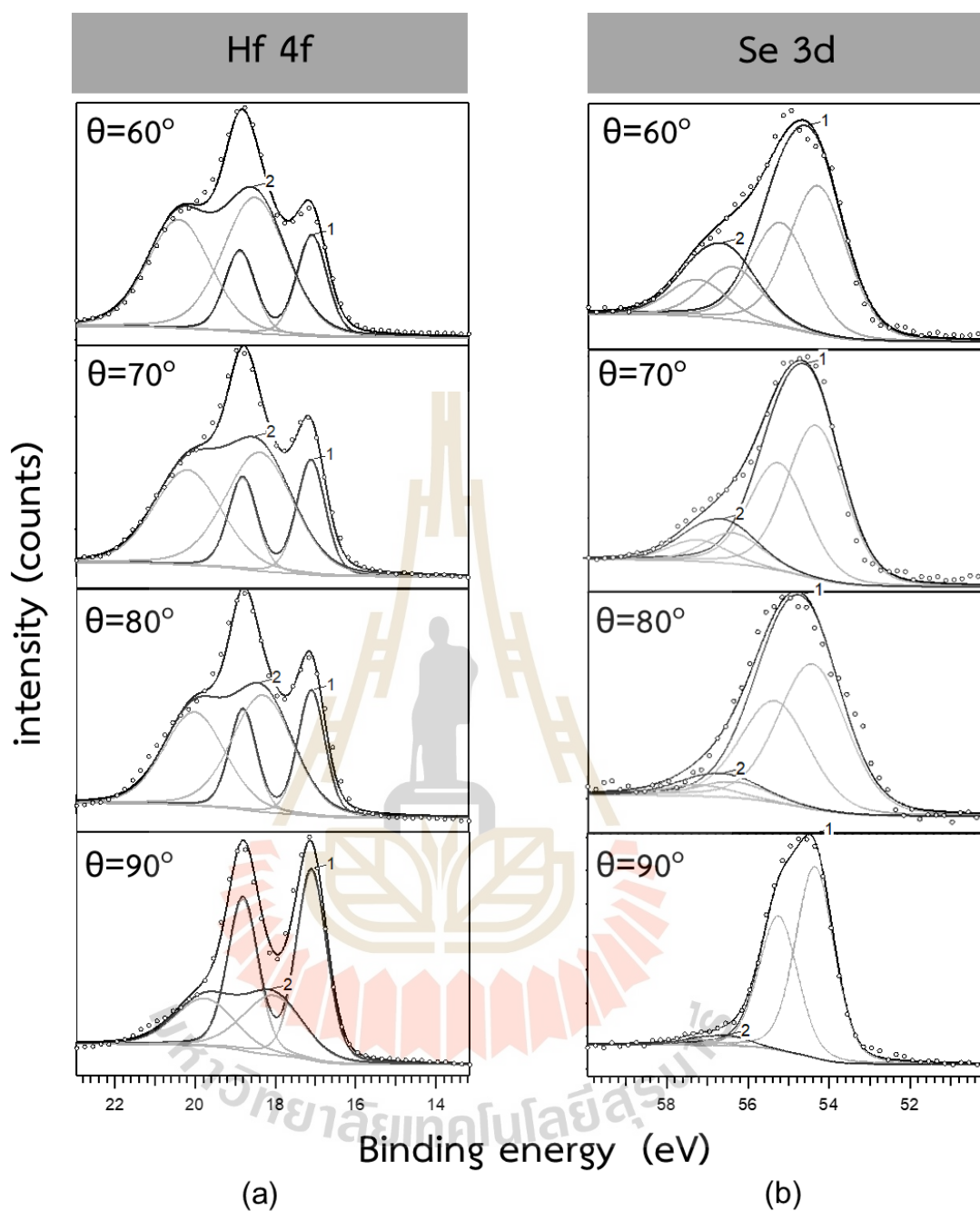


**Figure 4.1** XPS spectra (dot) and fits (lines) of (a) Hf 4f, (b) Se 3d of the  $\text{HfSe}_2$  after 1 day of ambient exposure with  $60^\circ$ ,  $70^\circ$ ,  $80^\circ$  and  $90^\circ$  take-off angles.

The deconvolution of the Se 3d photoelectron spectrum revealed that two chemical species, as shown in Figure 4.1(b), were assigned to Se-Hf by

the 1<sup>st</sup> doublet peak for Se 3d<sub>3/2</sub> at 55.23 and Se 3d<sub>5/2</sub> at 54.30 eV. The 2<sup>nd</sup> doublet peaks are assigned to a Se-Se chemical state with 3d<sub>3/2</sub> and 3d<sub>5/2</sub> at 57.39 eV and 56.52 eV, respectively.

When we change the takeoff angle, we will notice that the concentration of Hf 4f and Se 3d subpeak will change. According to the spectrum of the Hf 4f region, which is composed of HfSe<sub>2</sub> and HfO<sub>2</sub> components, the intensity of the Hf-Se peak increases with the angle and is more significant than the intensity of the Hf-O peak. This demonstrates that the HfO<sub>2</sub> is formed near the flake's surface. The Se 3d spectrum is composed of Se-Hf and Se-Se chemical states. These features are shown in Figure 4.1(b). There is an apparent relationship between the angle and the intensity of the Se-Se subpeaks. The decrease in Se-Se with angle implies that the Se-Se is dispersed in the upper region of the flake.

#### 4.1.2 Argon ion sputtering XPS depth profile

A sample of HfSe<sub>2</sub> exposed to the ambient was subjected to 4 keV Ar ion sputtering. Figure 4.2 shows the XPS depth profiles revealing the variation in peak area of Hf 4f and Se 3d spectra as a function of sputtering time.

These results reveal that after ambient exposure, the HfSe<sub>2</sub> surface is partially oxidized to HfO<sub>2</sub>. The high resolution Hf 4f spectra are deconvoluted into two doublet subpeaks which correspond to the binding energies of Hf-Se and Hf-O. For deconvoluted high resolution Se 3d spectra, two doublet subpeaks are detected that are assigned to Se-Hf and Se-Se.

After 1 minute of sputtering, we can see that the Hf-O subpeak has dropped, which has caused the Hf-Se subpeak to increase in concentration. After sputtering for 15 minutes, a new subpeak appears in the Hf 4f spectra. We observed that the Hf suboxide (Hf<sup>x+</sup>) doublet peak occurs at 16.4 eV for Hf 4f<sub>7/2</sub> and 18.1 eV for Hf 4f<sub>5/2</sub>. After Ar ion sputtering for 30 minutes, we can see that Hf-O subpeak are completely eliminated but Hf suboxide doublet peak appears to increase in the Hf 4f spectra. It shows that the studying of depth profile by Argon ion sputtering, which is destructive characterization approach, will produce chemical composition transforms

into Hf suboxide ( $\text{Hf}^{x+}$ ) which indicates that it is difficult to eliminate the  $\text{HfO}_2$  layer formed by the oxidation of  $\text{HfSe}_2$ .

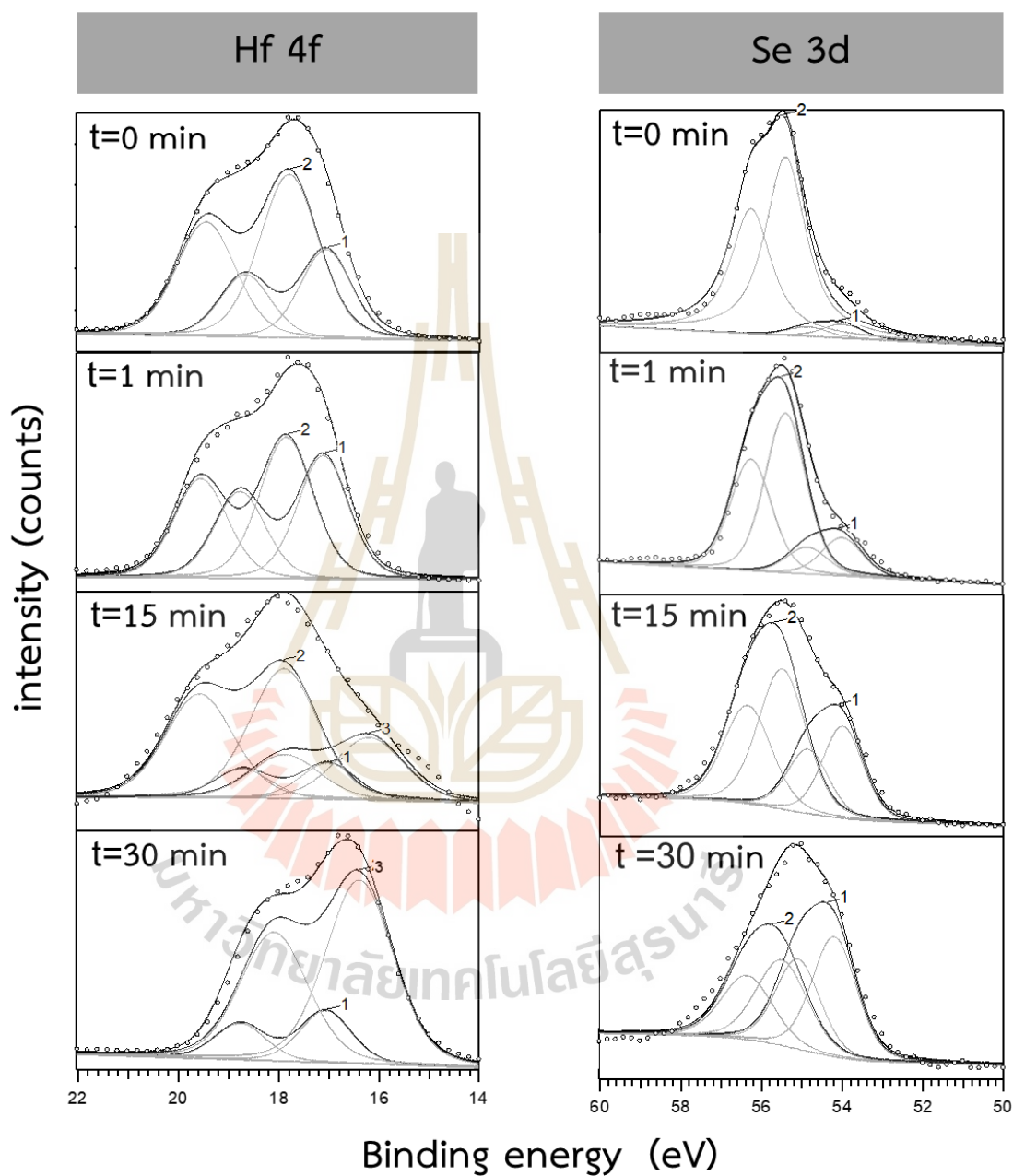


**Figure 4.2** XPS spectra (dot) and fits (lines) of (a) Hf 4f, (b) Se 3d of the  $\text{HfSe}_2$  after 1 day of ambient exposure before and after 1 min, 15 min, and 30 min of Ar ion sputtering.



The Se 3d spectra deconvolution confirms that Se-Se bonding is formed (which is a residual material) when the  $\text{HfSe}_2$  is oxidized to  $\text{HfO}_2$  where the Se-Se appears on the upper surface as observed by Se 3d spectra after ambient exposure. As the sputtering time is longer, Se-Se doublet subpeaks decrease continuously in concentration whereas Se-Hf doublet subpeaks increase since Ar ion sputtering eliminate the Se-Se bonding on the top layer.

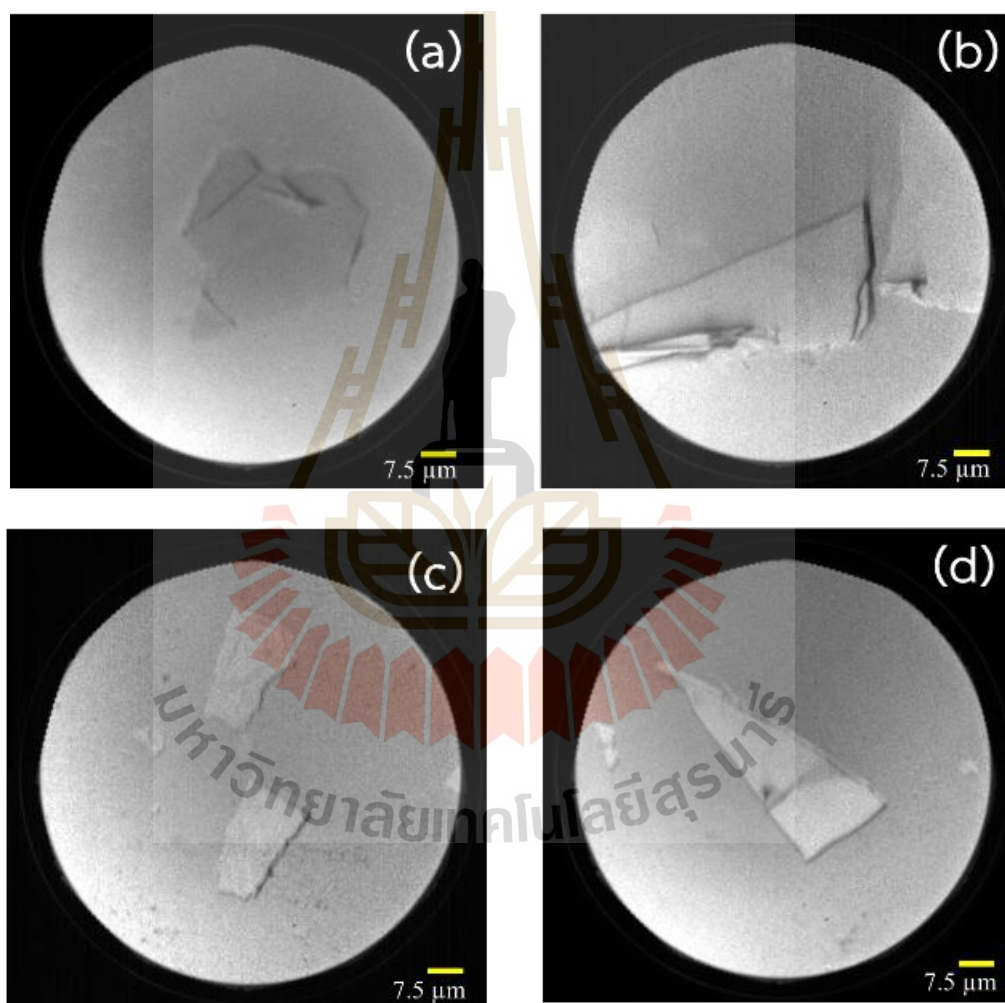


**Figure 4.3** PEEM images showing the pristine  $\text{HfSe}_2$  thin flakes for the surface oxidation dynamic by  $\text{H}_2\text{O}$  (a),  $\text{O}_2$  (b) exposed in vacuum pressure environment and air (c) and 95±5% RH (d) exposed in atmospheric pressure environment.

## 4.2 The surface oxidation dynamic of Hafnium Diselenide (HfSe<sub>2</sub>)

### 4.2.1 PEEM image of Hafnium Diselenide (HfSe<sub>2</sub>) thin flakes

PEEM images reveal micrometer-scale of pristine HfSe<sub>2</sub> thin flakes as shown in Figure 4.3(a) – (d), for investigating the dynamic of surface oxidation after the in-situ H<sub>2</sub>O and O<sub>2</sub> exposure in a vacuum pressure environment and the ex-situ air and 95±5% RH exposure in an atmospheric pressure environment.

### 4.2.2 Area probe X-ray Photoelectron Spectroscopy (Area probe-XPS)

The surface oxidation dynamic of hafnium diselenide was investigated by using the Area probe-XPS, a surface sensitive technique. The XPS spectra of Hf 4f and Se 3d core levels as a function of exposure time are shown in Figure 4.4; note that all spectra were calibrated using the Si 2p peak from underlying SiO<sub>2</sub> substrates. The pristine HfSe<sub>2</sub> thin flakes show Hf 4f in the lower panel represent to 1<sup>st</sup> doublet peaks attributed by the two peaks for Hf 4f<sub>5/2</sub> at ~18.79 eV and Hf 4f<sub>7/2</sub> at ~17.08 eV (Zhao et al., 2019).

The changes in the Hf 4f profile over exposure time indicate Hf oxidation. In-situ H<sub>2</sub>O exposure (Figure 4.4(a)) appears two new peaks indicate 2<sup>nd</sup> doublet peaks at 19.60 and 17.89 eV which correspond to the Hf 4f peaks for HfO<sub>2</sub> (Zhao et al., 2019) within 4 hours. We see the HfO<sub>2</sub> peak within 1-hour on in-situ O<sub>2</sub> exposure (Figure 4.4(b)). For the ex-situ air (Figure 4.4(c)) and 95±5% RH exposure (Figure 4.4(d)), a broadening of the spectra is observed due to the formation of the HfO<sub>2</sub>. For 4-hour exposure on Ex-situ by 95±5% RH exposure, we only see the peak of HfO<sub>2</sub>. This indicates that the top surface of HfSe<sub>2</sub> thin flake is fully oxidized.

The corresponding spectra of Se 3d core level for a time span of this exposure re shown in Figure 4.5. The pristine HfSe<sub>2</sub> for all exposure (lower panel) represents only 1<sup>st</sup> doublet peak located at ~55.16 eV and ~54.30 eV representing the Se 3d<sub>3/2</sub> and 3d<sub>5/2</sub> core levels respectively (Zhao et al., 2019). After Hf being oxidized by the in-situ H<sub>2</sub>O (Figure 4.5(a)) and in-situ O<sub>2</sub> (Figure 4.5(b)) exposures, we also detect emergence of two additional 3d peaks which indicate 2<sup>nd</sup> doublet peaks assigned to a Se-Se chemical state with 3d<sub>3/2</sub> at ~56.67 eV and 3d<sub>5/2</sub> at ~55.80 eV respectively

(Zhao et al., 2019). The intensity of these peaks increases over exposure time. The 2<sup>nd</sup> doublet peaks after the ex-situ air expose (Figure 4.5(c)) are weaker than ones from the in-situ exposure. For the ex-situ 95±5% RH exposure case (Figure 4.5(d)), we can only observe the 2<sup>nd</sup> doublet peaks after fully oxidized. The lack of SeO<sub>2</sub> spectra suggests that the oxidation happens only for HfO<sub>2</sub> and Se-Se bonding is a residual material arising from the HfO<sub>2</sub> formation.

From these results, it was found that H<sub>2</sub>O and O<sub>2</sub> exposure are the cause of HfSe<sub>2</sub> surface oxidation while the O<sub>2</sub> exposure gives the faster rate than the H<sub>2</sub>O exposure. A synergistic effect between H<sub>2</sub>O and O<sub>2</sub> is clearly observed for fully oxidized by 4-hour 95±5% RH exposure. On the contrary, the spontaneous oxidation under only one of H<sub>2</sub>O or O<sub>2</sub> exposure is partly oxidized on the HfSe<sub>2</sub> surface and still preserved for the Hf-Se bonding.

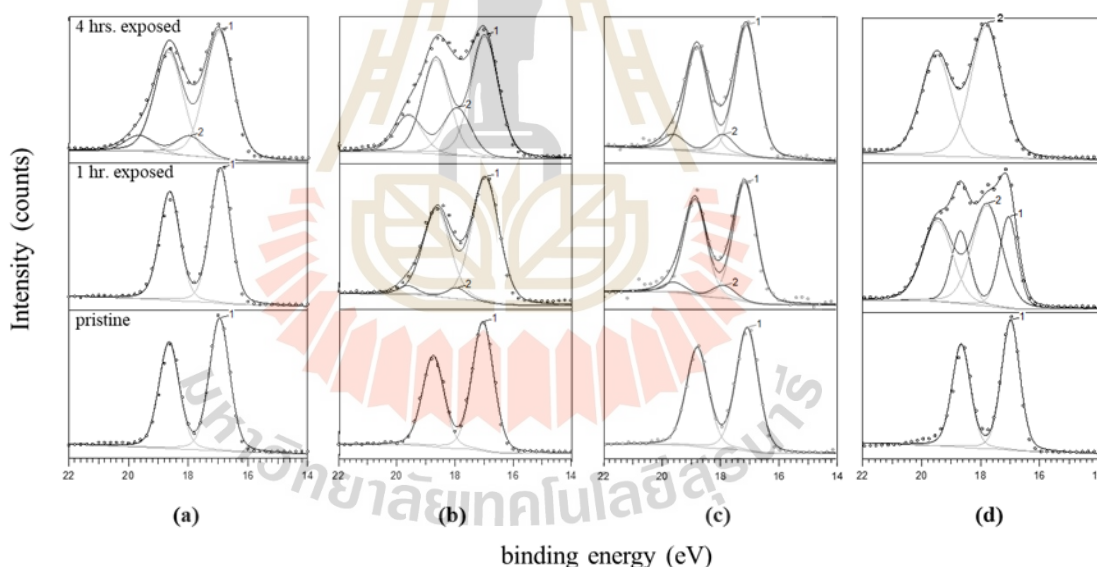


**Figure 4.4** Area probe-XPS spectra of Hf 4f peaks profile by In-situ H<sub>2</sub>O (a), In-situ O<sub>2</sub> (b), Ex-situ air (c) and Ex-situ 95±5% RH (d) exposure in pristine (lower panel), pristine (lower panel), 1 hour exposure (Middle panel), and 4 hours exposure (upper panel). Dot are experimental data. The 1<sup>st</sup> and 2<sup>nd</sup> doublet peaks are corresponding Lorentzian fit to Hf 4f peak for HfSe<sub>2</sub> and HfO<sub>2</sub> respectively.

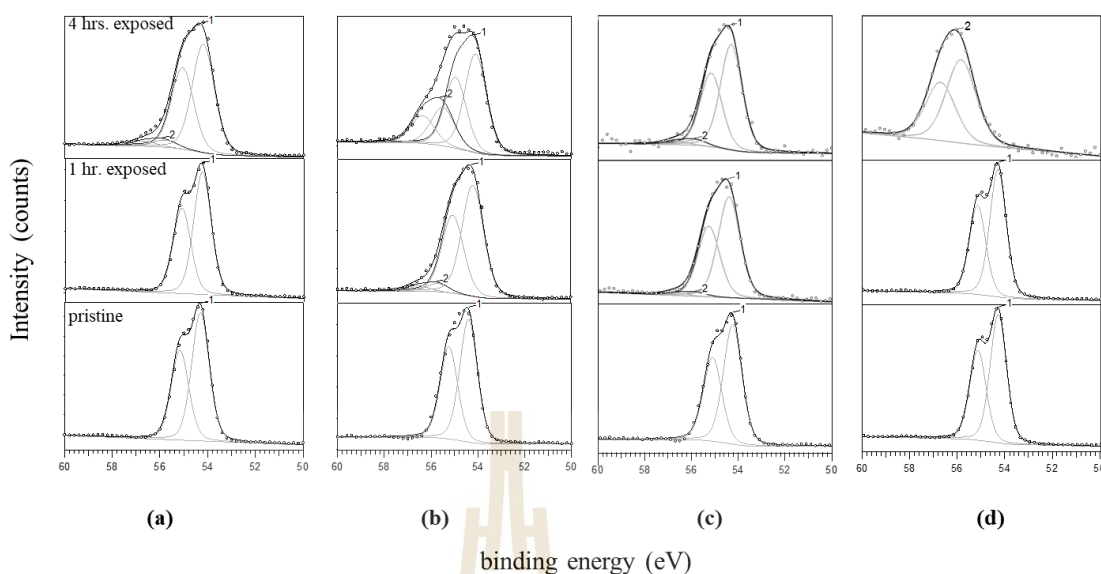


**Figure 4.5** Area probe-XPS spectra of Se 3d peaks profile by In-situ H<sub>2</sub>O (a), In-situ O<sub>2</sub> (b), Ex-situ air (c) and Ex-situ 95±5% RH (d) exposure in pristine (lower panel), 1 hour exposure (Middle panel), and 4 hours exposure (upper panel). Dots are experimental data. The 1<sup>st</sup> and 2<sup>nd</sup> doublet peaks are corresponding Lorentzian fit to 3d peak for HfSe<sub>2</sub> and Se-Se bonding respectively.

### 4.2.3 Work function Mapping

In order to see all the surface structure, we generated work function maps by fitting an error function to each pixel in the field of view, based on the low energy emission cutoffs from EF-PEEM images. Figure 4.6 represents the work function map evolution of the HfSe<sub>2</sub> thin flake that was recorded at the same position in 3 conditions: H<sub>2</sub>O, O<sub>2</sub> exposed in vacuum pressure, and 95±5% RH exposed in atmospheric pressure.

The work function mapping measurements in this experiment are relative measurements, that is, the SiO<sub>2</sub> substrate is used as a fixed reference value through measurement of the distinct cutoffs for the secondary electron spectra.

All the thin HfSe<sub>2</sub> flakes show very little inhomogeneity in work function in the area around the flake's convex folds because of their residing on surface defects as verified by microscopy. In pristine, we can clearly observe the work function contrast

of  $\text{SiO}_2$  and  $\text{HfSe}_2$ . Outlines that resemble grain boundaries can be clearly observed. After being exposed to 3 different conditions, this contrast persists but is attenuated with increasing exposure time. When the  $\text{HfSe}_2$  flake is exposed to  $\text{O}_2$  in a vacuum (Figure 4.6(b)), it takes less exposure time to see the attenuated work function contrast than when it is exposed to  $\text{H}_2\text{O}$  in a vacuum (Figure 4.6(a)). In particular, we can't see the work function contrast between  $\text{SiO}_2$  and  $\text{HfSe}_2$  after 4 hours exposed to  $95\pm 5\%$  RH at atmospheric pressure (Figure 4.6(c)).

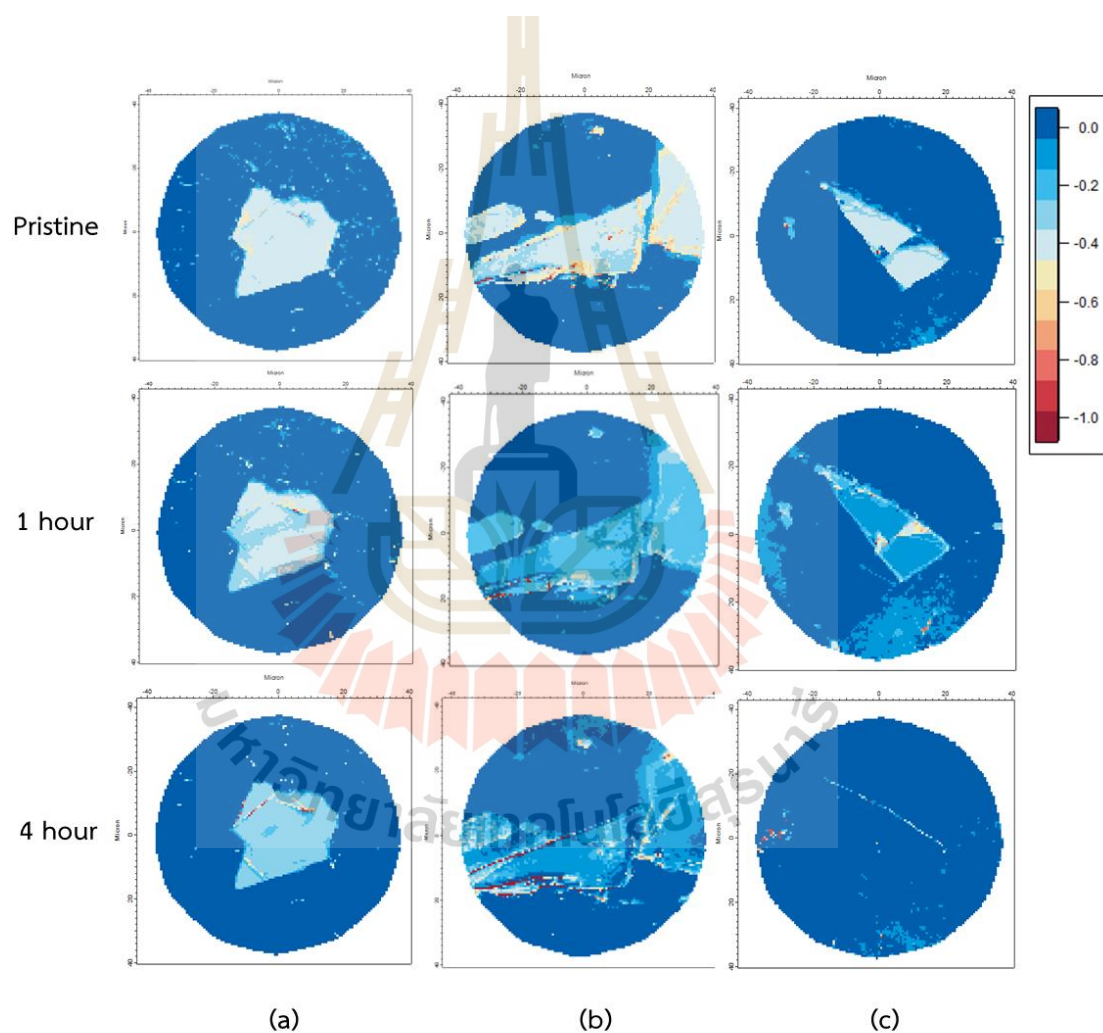


**Figure 4.6** PEEM measurements of the  $\text{HfSe}_2$  flakes work function mapping for In-situ  $\text{H}_2\text{O}$  (a), In-situ  $\text{O}_2$  (b), Ex-situ  $95\pm 5\%$  RH (c) exposure in pristine (upper panel), 1 hour exposure (middle panel), and 4 hours exposure (lower panel).

From the area probe-XPS results in section 4.2.2 show that surface oxidation of  $\text{HfSe}_2$  is a synergistic effect between  $\text{H}_2\text{O}$  and  $\text{O}_2$  where the  $\text{O}_2$  exposure will give oxidation rate faster than the case of  $\text{H}_2\text{O}$  exposure. This corresponds to the change in work function contrast. So, we propose that the difference in oxidation behavior and the difference work function contrast are both similar behaviors that seem to be linked.



## CHAPTER V

### CONCLUSION

#### 5.1 Conclusions

In this work, we study depth profile of HfSe<sub>2</sub> flake after ambient exposure. The results of the nondestructive technique with angle dependent measurement demonstrate that HfO<sub>2</sub> is maximum in the upper layer of HfSe<sub>2</sub> and decreases significantly with depth. The uppermost layer of the HfSe<sub>2</sub> surface also has the greatest concentration of the forming Se-Se combination. When destructive measurements are performed using argon sputtering, Hf-O and Se-Se are removed from the surface; however, Hf Suboxide (Hf<sup>x+</sup>) is produced when the sputtering is done.

The effects of oxidation on exfoliated flakes of HfSe<sub>2</sub> are investigated under various conditions, including exposure to O<sub>2</sub> and H<sub>2</sub>O in a vacuum, exposure to ambient and 95.5% relative humidity (RH) at atmospheric pressure. The study's results using photoemission electron microscopy (PEEM) with in-situ measurements indicate that H<sub>2</sub>O and O<sub>2</sub> both cause surface oxidation, from HfSe<sub>2</sub> to HfO<sub>2</sub>, with O<sub>2</sub> exposure causing stronger oxidation than H<sub>2</sub>O exposure. Complete oxidation of the surface and the formation of Se-Se bonding occur after 4 hours of exposure to 95±5% RH at atmospheric pressure. For fully oxidized, there is a strong synergistic effect between H<sub>2</sub>O and O<sub>2</sub>.

The oxide formation on the HfSe<sub>2</sub> surface described by the O atom is stronger electronegativity than Se. The resulting in the thermodynamically favorable process of the O replaces Se leads to susceptible oxidation. By using the model of chemical reactivity through density functional theory (DFT) on Palladium ditelluride (PdTe<sub>2</sub>), the theoretical results reveal that oxygen is energetically favorable by physical adsorption but unfavorable adsorption of water at room temperature, suggested by the differential Gibbs free energy. The underlying mechanism of the new Se-Se bonding is described by that the oxygen comes into play in oxidation process and the preferential

formation of Hf oxidation produces Se atom in a residual material. The Se atom is favorable to form Se–Se bonding than Se–O because estimated bond energies by Pauling equation indicates that the Se–Se uses lower covalent bond energy than Se–O (172 versus 233 kJ/mol). This is in agreement that the formation of Se oxide is not detected experimentally.

In this experiment, the work function mapping measurements are made relative to the SiO<sub>2</sub> substrate by measuring the absolute value of the secondary electron cutoffs. The work function mapping of HfSe<sub>2</sub> under various conditions demonstrates that the contrast remains after exposure. As exposure time increases, the persistence of work function contrast becomes less apparent and different for each condition. Consequently, we propose that the difference in oxidation behavior and the difference in work function contrast are both linked behaviors that appear to be related.

## 5.2 Future direction

At this stage, we properly understand the oxidation process of HfSe<sub>2</sub>. Thus, we will fabricate FETs based on hafnium diselenide (HfSe<sub>2</sub>) that create a thin layer of HfO<sub>2</sub> that is oxidized from HfSe<sub>2</sub> as a gate insulator in the future.



REFERENCES

มหาวิทยาลัยเทคโนโลยีสุรนารี

## REFERENCES

- Azcatl, A., McDonnell, S., Santosh, K. C., Peng, X., Dong, H., Qin, X., ... Wallace., R.M. (2014). MoS<sub>2</sub> functionalization for ultra-thin atomic layer deposited dielectrics. *Appl. Phys. Lett*, *104*, 111601. doi:10.1063/1.4869149.
- Azo materials (2020). Using XPS to Map the Work Function of a Damaged Solar Cell. Retrieved from <https://www.azom.com/article.aspx?ArticleID=19270>.
- Barrett, N., and Renault, O. (2009). La spectromicroscopie XPEEM avec le rayonnement synchrotron. *Mater. Tech.*, *97*(2), 101-122.
- Chhowalla, M., Shin, H.S., Eda, G., Li, L.-J., Loh, K.P., and Zhang, H. (2013). The chemistry of two-dimensional layered transition metal dichalcogenide nanosheets. *Nat. Chem*, *5*, 263–275. doi:10.1038/nchem.1589.
- Cruz, A., Mutlu, Z., Ozkan M., and Ozkan, C.S. (2018). Raman investigation of the air stability of 2H polytype HfSe<sub>2</sub> thin films. *MRS Communications*, *8*(3), 1191–1196. doi:10.1557/mrc.2018.185.
- Frégnaux, M., Kim, H., Rouchon, D., Derycke, V., Bleuse, J., Voiry, D., ... Renault, O. (2016). Chemistry and electronics of single layer MoS<sub>2</sub> domains from photoelectron spectromicroscopy using laboratory excitation sources. *Surf. Interface Anal.*, *48*, 465-439.
- Geim, A., and Novoselov K. (2007). The rise of graphene. *Nature Materials*, *6*, 183–191. doi:10.1038/nmat1849.
- Greiner, M. (2016). Photoelectron spectroscopy investigation of Oligoaniline-iron oxide interfaces for understanding corrosion inhibition (Master dissertation, McMaster University) Retrieved from [https://macsphere.mcmaster.ca/bitstream/11375/21584/1/Greiner\\_Mark\\_2007Dec\\_Masters.pdf](https://macsphere.mcmaster.ca/bitstream/11375/21584/1/Greiner_Mark_2007Dec_Masters.pdf).
- Jablonski, A., and Powell, C.J. (2002). The electron attenuation length revisited. *Surface Science Reports*, *47*(2–3), 33-91. doi:10.1016/S0167-5729(02)00031-6.

- Kaja, K. (2010) Development of nano-probe techniques for work function assessment and application to materials for microelectronics. (Doctoral dissertation, Université Joseph-Fourier - Grenoble) Retrieved from <https://tel.archives-ouvertes.fr/tel-00515370/document>.
- Kanazawa, T., Amemiya, T., Ishikawa, A., Upadhyaya, V., Tsuruta, K., Tanaka, T., and Miyamoto, Y. (2016). Few-layer HfS<sub>2</sub> transistors. *Sci Rep*, 6, 22277. doi:10.1038/srep22277.
- Kang, M., Rathi, S., Lee, I., Lim, D., Wang, J., Li, L., ... Kim, G-H. (2015). Electrical characterization of multilayer HfSe<sub>2</sub> field-effect transistors on SiO<sub>2</sub> substrate. *Appl. Phys. Lett.* 106, 143108. doi:10.1063/1.4917458.
- Kang, M., Rathi, S., Lee, I., Li, L., Khan, M.A., Lim, D., ... Kim, G.H. (2017). Tunable electrical properties of multilayer HfSe<sub>2</sub> field effect transistors by oxygen plasma treatment. *Nanoscale*. 9(4), 1645–1652. doi:10.1039/C6NR08467B.
- Koopmans, T. (1934). Über die Zuordnung von Wellenfunktionen und Eigenwerten zu den einzelnen Elektronen eines Atoms. *Physica*, 1(1–6), 104–113.
- Liu, L., Li, Y., Huang, X., Chen, J., Yang, Z., Xue, K-H., ... Miao, X. (2021). Low-Power Memristive Logic Device Enabled by Controllable Oxidation of 2D HfSe<sub>2</sub> for In-Memory Computing. *Advanced Science*, 8, 2005038. doi:10.1002/advs.202005038.
- McDonnell, S., Brennan, B., Azcatl, A., Lu, N., Dong, H., Buie, C., ... Wallace, R.M. (2013). HfO<sub>2</sub> on MoS<sub>2</sub> by atomic layer deposition: adsorption mechanisms and thickness scalability. *ACS Nano*. 7(11), 10354–61. doi: 10.1021/nn404775u.
- Mirabelli, G., McGeough, C., Schmidt, M., McCarthy, E.K., Monaghan, S., Povey, I.M., ... Duffy, R. (2016). Air sensitivity of MoS<sub>2</sub>, MoSe<sub>2</sub>, MoTe<sub>2</sub>, HfS<sub>2</sub>, and HfSe<sub>2</sub>. *Journal of Applied Physics*, 120, 125102. doi:10.1063/1.4963290.
- Mleczko, M.J., Zhang, C., Lee, H.R., Kuo, H-H., Magyar-Köpe, B., Moore, R.G., ... Pop, E., (2017). HfSe<sub>2</sub> and ZrSe<sub>2</sub>: Two-dimensional semiconductors with native high-κ oxides. *Science Advances*. 3(8), e170048. doi:10.1126/sciadv.1700481.

- Pankove, J.I. (1975). *Optical Processes in Semiconductors*. New York: Dover Publications, Inc.
- Powell, C., and Jablonski, A. (1999). NIST Electron Inelastic-Mean-Free-Path Database 71, Version 1.0, Nat'l Std. Ref. Data Series (NIST NSRDS), National Institute of Standards and Technology, Gaithersburg, MD (Accessed November 11, 2021).
- Radisavljevic, B., Radenovic, A., Brivio, J., Giacometti, V., and Kis, A. (2011). Single – layer MoS<sub>2</sub> transistors. *Nat Nanotechnol.* 6(3), 147-50. doi:10.1038/nnano.2010.279).
- Renault, O., Garnier, A., Morin, J., Gambacorti, N., and Bertin, F. (2012). High-resolution XPS spectromicroscopy study of micro-patterned gold–tin surfaces. *Applied Surface Science*, 285, 10077-10083. doi:10.1016/j.apsusc.2012.06.078.
- Schneider, T., Artyushkova, K., Fulghum, J.E., Broadwater, L., Smith, A., and Lavrentovich O.D. (2005). Oriented Monolayers Prepared from Lyotropic Chromonic Liquid Crystal. *American Chemical Society*, 21(6), 2300-2307. doi.org/10.1021/la047788+.
- Stohr, J., and Anders, S. (2000). X-ray spectro-microscopy of complex materials and surfaces. *IBM Journal of Research and Development*, 44(4), 535-551. doi: 10.1147/rd.444.0535.
- Sowinska, M. (2014). In-operando hard X-ray photoelectron spectroscopy study on the resistive switching physics of HfO<sub>2</sub>-based RRAM (Master dissertation, Brandenburg University of Technology Cottbus - Senftenberg). Retrieved from [https://opus4.kobv.de/opus4-btu/files/3007/Malgorzata\\_Sowinska.pdf](https://opus4.kobv.de/opus4-btu/files/3007/Malgorzata_Sowinska.pdf).
- Tunmee, S. (2016). Synchrotron - Based Spectromicroscopy and Electrochemical-Mechanical Analyses of Films of Diamond- Like Carbon and Related Materials (Doctoral dissertation, Nagaoka University of Technology). Retrieved from <https://nagaokaut.repo.nii.ac.jp>.

- Wlegmann, L. (1972). The photo-emission electron microscope: Its technique and applications. *Journal of Microscopy*, *96*, 1-23. doi:10.1111/j.13652818.1972.tb03739.x.
- Xu, K., Huang, Y., Chen, B., Xia, Y., Lei, W., Wang, Z., ... He, J. (2016). Toward high-performance top-gate ultrathin HfS<sub>2</sub> field-effect transistors by interface engineering. *Small* *12*, 3106-3111. doi: 10.1002/sml.201600521.
- Yao, Q., Zhang, L., Bampoulis, P., and Zandvliet, H.J. (2018). Nanoscale Investigation of Defects and Oxidation of HfSe<sub>2</sub>. *The Journal of Physical Chemistry C*, *122*, 25498-25505. doi:10.1021/acs.jpcc.8b08713.
- Yasufuku, H., Yoshikawa, H., Kimura, M., Vlaicu, A.M, Kato, M., Kudo, M., ... Fukushima, S. (2006). On the wide-energy-range tuning of x-ray photoemission electron microscope optics for the observation of the photoelectrons excited by several keV x-rays. *Review of Scientific Instruments*, *77*, 033702. doi: 10.1063/1.2185493.
- Yin, L., Xu, K., Wen, Y., Wang, Z., Huang, Y., Wang, F., ... He, J. (2016). Ultrafast and ultrasensitive phototransistors based on few-layered HfSe<sub>2</sub>. *Appl. Phys. Lett.* *109*, 213105. doi:10.1063/1.4968808.
- Zborowski, C. (2018). Characterization of deeply buried interfaces by Hard X-ray Photoelectron Spectroscopy (Doctoral dissertation, University of Lyon and University of Southern Denmark). Retrieved from <https://www.theses.fr/2018LYSEC025/abes>.
- Zhao, L., Wei, Y., Zhang, R., and Peng, Y. (2019). Controlled surface oxidation of HfSe<sub>2</sub> via oxygen-plasma treatment. *Materials Letters*, *243*, 96-99. doi:10.1016/j.matlet.2019.02.024.
- Zou, K., Hong, X., Keefer D., and Zhu, J. (2010). Deposition of high-quality HfO<sub>2</sub> on graphene and the effect of remote oxide phonon scattering. *Physical review letters*, *105*(12), 126601. doi:10.1103/PhysRevLett.105.126601.

## CURRICULUM VITAE

**Name** Mr. Suwat Thila

**Date of birth** January 27th, 1995

**Place of birth** 56 Moo.6, Paka Village, Mae Raeng Sub-district,  
Pa Sang District, Lamphun Province, Thailand.

**Education**

2015-2022 **Master of Science (Physics): M.Sc. (Physics)**  
Suranaree University of Technology, Nakhon Ratchasima,  
Thailand.

2013-2016 **Bachelor of Science (Physics): B.Sc. (Physics)**  
Naresuan University, Phitsanulok, Thailand.

**Grants and Fellowships** Development and Promotion of Science and Technology  
Talents Project, Thai government scholarship (DPST)

**Publications**  
Suwat Thila, Thipusa Wongpinij, Pakwan Chanprakhon, Narong Chanlek, Chanan  
Euaruksakul and Worawat Meevasana. In-situ and Ex-situ study of oxidation at  
the surface of hafnium diselenide  $\text{HfSe}_2$ , Present at The 21<sup>st</sup> International  
Union of Materials Research Societies-International Conference in Asia  
(IUMRS-ICS 2020), Thailand (2021-02-23–2021-02-26)